Methylotrophic methanogenesis in the Archaeoglobi: Cultivation of *Ca.* Methanoglobus hypatiae from a Yellowstone hot spring

Mackenzie M. Lynes[1], Zackary J. Jay[1], Anthony J. Kohtz[1], Roland Hatzenpichler[1,2,*]

[1] Department of Chemistry and Biochemistry, Center for Biofilm Engineering, and Thermal Biology Institute, Montana State University, Bozeman, MT 59717, USA
[2] Department of Microbiology and Cell Biology, Montana State University, Bozeman, MT 59717, USA
[*] Corresponding author: Roland Hatzenpichler, email: roland.hatzenpichler@montana.edu

ORCID Numbers of Authors: M.M.L., 0000-0002-9410-0285; Z.J.J., 0000-0003-3062-4933; A.J.K., 0000-0002-0561-8710; R.H, 0000-0002-5489-3444
Competing Interest Statement: none declared.

Abstract

Over the past decade, environmental metagenomics and PCR-based marker gene surveys have revealed that several lineages beyond just a few well-established groups within the Euryarchaeota superphylum harbor the genetic potential for methanogenesis. One of these groups are the Archaeoglobi, a class of obligately thermophilic Euryarchaeotes that have long been considered to live a non-methanogenic lifestyle. Here, we enriched *Candidatus* Methanoglobus hypatiae, a methanogen affiliated with the family Archaeoglobaceae, from a hot spring in Yellowstone National Park. The enrichment is sediment-free, grows at 64-70 ºC and a pH of 7.8, and produces methane from mono-, di-, and tri-methylamine. *Ca.* M. hypatiae is represented by a 1.62 Mb metagenome-assembled genome with an estimated completeness of 100% and accounts for up to 67% of cells in the culture according to fluorescence *in situ* hybridization. Via genome-resolved metatranscriptomics and stable isotope tracing, we demonstrate that *Ca.* M. hypatiae expresses methylotrophic methanogenesis and energy-conserving pathways for reducing monomethylamine to methane. The detection of Archaeoglobi populations related to *Ca.* M. hypatiae in 36 geochemically diverse geothermal sites within Yellowstone National Park (pH 2.61-9.35; 18.4 to 93.8 ºC), as revealed through the examination of previously published gene amplicon datasets, implies a previously underestimated contribution to anaerobic carbon cycling in extreme ecosystems.

Significance statement

The majority of global methane emissions are attributed to the activity of methane-producing anaerobic archaea, the methanogens. Over the last decade, environmental DNA sequencing demonstrated that culture collections do not adequately represent the true taxonomic and metabolic diversity of methanogens present in nature. One group of archaea postulated to contribute to methane production in high temperature marine and terrestrial environments are the Archaeoglobi, a group of obligate thermophilic archaea within the Euryarchaeota superphylum. Here, we report the cultivation and physiological characterization of a methanogenic member of the Archaeoglobi, *Ca.* Methanoglobus hypatiae, from a hot spring in Yellowstone National Park. Via a combination of growth experiments, stable isotope tracing, metatranscriptomics, microscopy analyses, and re-examination of gene amplicon surveys, our study provides direct experimental evidence of methanogenesis in the Archaeoglobi and shows that closely related archaea are widely distributed in Yellowstone's geothermal features.

Introduction

Methanogenesis is one of the most ancient metabolic pathways and plays a major role in the biogeochemical carbon cycle. Phylogenomic reconstructions and geological evidence suggest that methanogenesis was among the earliest metabolisms to evolve and that the last common ancestor of all extant archaea likely was a methanogen (1-9). Therefore, the study of methanogens is essential for understanding the co-evolution of life and the biosphere. Methanogenic archaea are the primary producers of biogenic methane (CH_4) and contribute approximately 60% to the estimated 576 Tg of annual global methane emissions to the atmosphere (10, 11). Methanogenic pathways are classified based on the specific substrate that is reduced to produce methane (12-14). All methanogenic pathways converge at the terminal methane-forming step catalyzed by the methyl-coenzyme M reductase (MCR) complex. MCR and its homologs also catalyze the reversible reaction in the anaerobic oxidation of alkanes in alkanotrophic archaea (15, 16). MCR is uniquely present in all methanogens and is commonly used to identify potential methane and/or alkane cycling archaea in sequencing surveys (12, 17).

The physiology and biochemistry of methanogens has near-exclusively been investigated in axenic cultures of microorganisms belonging to the Euryarchaeota superphylum (12, 17-19). These predominantly grow by aceticlastic or CO_2-reducing hydrogenotrophic methanogenesis, with limited observations of Euryarchaeota exclusively using methylated precursors (12, 20, 21). As a result, methylotrophic methanogenesis was considered to be of very limited environmental distribution. The extensive use of environmental metagenomics has led to the discovery of metagenome-assembled genomes (MAGs) encoding MCR from new lineages that are prevalent in anoxic environments, both within and outside the Euryarchaeota (2, 12, 22-26).

The majority of MAGs affiliated with archaeal phyla outside the Euryarchaeota are predicted to be methyl-reducing methanogens, with the exception of *Candidatus* (*Ca.*) Nezhaarchaeota (25, 27) and *Ca.* Methanomixophus affiliated with the order Archaeoglobales, which have been hypothesized to be CO_2-reducing hydrogenotrophic methanogens (12, 25, 28). This result is consistent with the observation that methylated methanogenic substrates, including different methylamines and methanol, are prevalent in the environment, although their concentrations in hot springs is currently unknown. Further, methyl-reducing methanogenesis is considered the predominant mode of methanogenesis in anoxic marine, freshwater, and hypersaline sediments (reviewed in (20)).

Members of the class Archaeoglobi have long been considered non-methanogenic with isolates characterized as dissimilatory sulfate reducers brought into culture as early as 1987 (29). To date, only nine species of the class Archaeoglobi have been obtained in axenic culture, and all were sourced from marine hydrothermal systems or off-shore oil reservoirs (30). The discovery of both MCR (25, 31, 32) and methyl-H_4M(S)PT:coenzyme M methyltransferase (MTR) complexes in genomes of the Archaeoglobaceae have suggested that members of this family may live by methanogenesis rather than by sulfate reduction (28).

Very recently, important progress towards experimental verification of methanogenesis by members of this family has been made. Liu *et al.* reported the *in situ* expression of genes related to hydrogen-dependent methylotrophic methanogenesis and heterotrophic fermentation within populations of Archaeoglobi in a high-temperature oil reservoir (28). Lynes, Krukenberg *et al.* reported that Archaeoglobi can be enriched in hot spring mesocosms under methanogenic conditions (33). Wang *et al.* reported that *mcrABG* and other methanogenesis marker genes encoded by two Archaeoglobales MAGs were highly expressed in hot spring microcosms incubated at 65 ºC and 75 ºC (34). Importantly, one of these Archaeoglobales MAGs represented the only Mcr-encoding archaeon that expressed *mcrABG* genes in methanogenic microcosms performed without substrate addition or with the addition of 10 mM methanol

at 75 ºC. This indirectly demonstrated the methanogenic nature of this archaeon (34). Last, Buessecker *et al.* reported the establishment of a methanogenic enrichment culture of *Ca.* Methanoglobus nevadensis from Great Boiling Spring (NV, USA) (35). The culture yields up to 158 µmol of methane per liter after two weeks of incubation at its optimal growth temperature of 75 ºC. *Ca.* M. nevadensis is represented by a 63% complete MAG obtained from the culture (35).

Here, we report on the enrichment cultivation of *Ca.* Methanoglobus hypatiae LCB24, a methanogen affiliated with the family Archaeoglobaceae, from a hot spring in Yellowstone National Park (YNP). Using a combination of targeted cultivation, growth experiments, microscopy, stable isotope tracing, metagenomics, and metatranscriptomics, we demonstrate that *Ca.* M. hypatiae lives by methylotrophic methanogenesis and converts different methylamines to methane. By examining previously published datasets for the presence of Mcr-encoding Archaeoglobi, we demonstrate that these archaea are distributed in geothermal features of YNP, where they likely contribute to anaerobic carbon cycling. Our study represents the first direct experimental evidence of a methanogen within the Archaeoglobaceae and adds to the growing body of evidence demonstrating that methanogenesis is widely spread within the Euryarchaeota superphylum.

Results and Discussion

Cultivation

In our recent survey on the diversity of Mcr-encoding archaea in the geothermal features of YNP, mesocosms seeded with biomass from a hot spring located within the Lower Culex Basin (LCB024; pH 7-8, 56-74 ˚C), had shown potential to enrich for methanogenic Archaeoglobi (33). Using a sediment slurry collected from LCB024, we initiated incubations supplied with monomethylamine (MMA) and antibiotics incubated in anoxic media (pH 7.8, 70 ˚C) under a N_2 headspace. The relative abundance, as determined by 16S rRNA gene amplicon sequencing, of Archaeoglobi-affiliated organisms in LCB024 was 0.32% in the initial slurry and had fallen to 0.02% by the time incubations were initiated a few months after samples had been collected (Fig. 1A).

Methane was detected after 36 days in the initial enrichment and the culture transferred to fresh media after reaching the late exponential phase of methane production following 70 days of incubation (447 µM; Fig. 1B). Five Archaeoglobi related 16S rRNA gene amplicon ASVs were identified in the initial enrichment, however one ASV grew to dominate the microbial community after the first transfer and reached 74.8% relative abundance after 62 days. In the transfers that followed, Archaeoglobi-related sequences became the only archaeal reads detected by 16S rRNA gene amplicon sequencing with the second most abundant organism a bacterium affiliated with the *Pseudothermotoga* at 6.80%. While the CO_2-reducing methanogen *Methanothermobacter* sp. was detected at 0.45% relative abundance in the slurry material used for inoculation, it was not detected in any subsequent transfers, nor were any other methanogens. Over subsequent transfers (238 days, T2-T5), the relative abundance of Archaeoglobi ASVs ranged from 46 to 69% and the final methane yield steadily increased from 1,844 to 2,459 µM. A sediment-free enrichment was obtained by the third transfer. Starting with the fourth transfer, the culture volume was scaled from 30 mL to 50 mL and designated as culture LCB24. By the sixth transfer, the culture produced 3,943 µM methane within 34 days. Metagenomic sequencing at two timepoints (day 335 of the enrichment and day 33 of the isotope tracing experiment described below) and 16S rRNA gene amplicon sequencing over recurring transfers (Fig. 1A) demonstrated that ASVs and MAGs affiliated with Archaeoglobi represented the only archaeon in culture LCB24. A single Mcr complex (*mcrAGCDB*) belonging to the

Archaeoglobi MAG was present, indicating this MAG exclusively represented the only population with methanogenic potential.

Metagenomics and Phylogenetics

The reconstructed LCB24 MAG of the Mcr-encoding archaeon was 1.62 Mbp in length with an estimated completeness of 100% according to checkM (SI Appendix, Table S3). This MAG was the result of a combined assembly of the T4-MG and SIT-MG genomes as this method yielded an improved assembly. Therefore, it was used for phylogenomic analysis against Archaeoglobi reference MAGs and genomes using 33 conserved single copy marker proteins and 16S rRNA genes (Fig. 2AB, SI Appendix, Table S4). Interestingly, MAGs that encoded Mcr complexes exhibited distinct clustering when assessed using a set of marker proteins, setting them apart from those lacking *mcr* gene sequences. Consistently, 16S rRNA gene phylogeny supported this clustering with a pronounced separation of reference genomes and MAGs based on geographical origin, resulting in three main clusters: (i) those retrieved from North American hot springs (YNP and Great Boiling Spring, GBS), (ii) those originating from hot springs in China, and (iii) those obtained from deep-sea marine hydrothermal systems (Fig. 2B). The examination of conserved marker proteins also revealed two distinct clades of Archaeoglobi within YNP features, categorized by the presence or absence of Mcr complexes.

LCB24 and closely related reference MAGs and isolate genomes exhibited a range of amino acid identities (AAI, 52.6-98.6%; Fig. 2C). Altogether, the LCB24 MAG was found to be highly related to previously obtained Archaeoglobi MAGs encoding the MCR complex and only distantly related to confirmed sulfate-reducing Archaeoglobales (AAI, 58.9-65%; ANI, 70.3-70.6%; 16S rRNA ANI, 91.6-93.8%; SI Appendix Fig. S1, S2). Based on AAI, MAG LCB24 was most closely related to Archaeoglobi LCB024-003 MAG (AAI, 98.6%), which we had obtained from the same hot spring in a previous study (33). The ANI and AAI values to the closest cultured methanogen, *Ca.* Methanoglobus nevadensis GBS, are 80.2 and 83.3%, respectively. Based on these results, we designate this archaeon *Ca.* Methanoglobus hypatiae strain LCB24, named after the philosopher Hypatia of Alexandria (for a protologue, see the SI Appendix, Results and Discussion). The estimated relative abundance of *Ca.* M. hypatiae based on the SIT-MG was 92.8%. Other community members in the LCB24 culture with >1% relative sequence abundance included members of the *Pseudothermotoga* (3.2%), *Desulfovirgula* (1.7%), and the family Moorellaceae (1.3%) (Fig. 1A, Dataset S1).

The only *mcrAGCDB* genes recovered from both metagenomes belong to the genome of *Ca.* M. hypatiae. Phylogenetic analysis of the single copy of McrA indicated its close relationship to McrA sequences found in members of the TACK superphylum (Fig. 2D). This contrasts with the placement of *Ca.* M. hypatiae within the Euryarchaeota based on phylogenomics (Fig. 2A), suggesting that Archaeoglobi could have obtained the Mcr complex as a result of a horizontal gene transfer event from an archaeon in the TACK superphylum (7, 8). Alternatively, it could indicate that non-methanogenic Archaeoglobi lost the capacity for anaerobic methane cycling after they had diverged from a shared methanogenic ancestor.

Methanogenic Activity of *Ca.* M. hypatiae

To gain insight into the activity of *Ca.* M. hypatiae under methanogenic and non-methanogenic conditions, a stable isotope tracing (SIT) experiment was conducted. Cultures were incubated in the presence of 10 mM of MMA; 8 mM of substrate were isotopically light, while the remaining 2 mM consisted of either ^{13}C-monomethylamine ($^{13}CH_3$-NH_2) or D_3-monomethylamine (CD_3-NH_2). Addition of the methanogenesis inhibitor bromoethanesulfonate (BES) was used as a non-methanogenic control (Fig.

1B, 3, SI Appendix, Fig. S3). On average across six replicates, the cultured converted $^{13}CH_3$-NH_2 to 356 μM $^{13}CH_4$ (17.8%) and 138.71 μM $^{13}CO_2$ (6.9%) by day 32 (Fig. 3AC, Dataset S2). The conversion of CD_3-NH_2 was nearly identical yielding 355 μM CD_3H (Fig. 3B). In the exponential phase of methane production, five of the six replicates were harvested for metagenomic and metatranscriptomic sequencing while the sixth replicate was allowed to grow to stationary phase. The replicate allowed to grow in each respective experiment converted the provided $^{13}CH_3$-NH_2 to 717.7 μM $^{13}CH_4$ (35.9%) and 212.95 μM $^{13}CO_2$ (10.65%) or CD_3-NH_2 to 394.76 μM CD_3H (19.7%) by day 38 (Fig. 3ABC). These results confirmed monomethylamine was converted to methane by the LCB24 culture. The production of $^{13}CO_2$ may represent the dismutation of $^{13}CH_3$-NH_2 to generate reducing power for methanogenesis via the methyl-branch of the Wood-Ljungdahl pathway or may be explained by other organisms in the culture catabolizing MMA. Yet, no transcriptomic evidence for this activity was present in this experiment. No methane production was observed for cultures treated with BES or in cultures incubated without MMA (Fig. 3D). When BES was added to cultures in the exponential phase, methane production ceased indicating the generation of methane is reliant on the Archaeoglobi MCR (Fig. 3E).

Visualization and cell enumeration

The growth of *Ca.* M. hypatiae was tracked in four replicates during the SIT experiment with catalyzed reporter deposition fluorescence *in situ* hybridization (CARD-FISH) using a general archaea-targeted probe Arch915 (36) and DNA-staining (DAPI) (Fig. 1C). As the production of methane increased throughout the experiment, there was a concurrent rise in the relative cell abundance of *Ca.* M. hypatiae (Fig. 3F, SI Appendix, Table S5). The initial assessment on day 22 across four replicates revealed the total cell density to be $3.45 \times 10^7 \pm 1.14 \times 10^7$ before substantial concentrations of methane had been detected in the headspace (<132 μM). By day 32, methane concentrations reached 1,777±739 μM and the total cell density increased to $6.97 \times 10^7 \pm 3.73 \times 10^7$ cells mL^{-1} with 54% (±9.6%) of cells labeled as *Ca.* M. hypatiae (Fig. 3F). All but one of these replicates were then sacrificed for further analysis. Finally on day 45, the remaining replicate reached a headspace methane concentration of 4,109 μM and a total cell density of 1.22×10^8 with 53% of cells labeled as *Ca.* M. hypatiae.

Visualization of the enrichment culture via scanning electron microscopy (SEM) revealed that most cells exhibited a regular to irregular coccoid morphology, with a width ranging from 0.5-1 μm (Fig. 1D). This morphology has previously been described for other Archaeoglobi species (30, 37-39).

Alternative Substrates and Temperature Optimum

We determined the substrate and temperature range of *Ca.* M. hypatiae by growing the culture in the presence of several substrates at 70 ºC or with 10 mM MMA at 60-85 ˚C (Fig. 4AB). Conditions that lead to the production of methane included 10 mM trimethylamine (TMA), 10 mM dimethylamine (DMA), 10 mM MMA in media without yeast extract, and the control with 10 mM MMA and 0.01% yeast extract. Methane production of cultures grown with MMA in the presence or absence of yeast extract were indistinguishable (5,202±606 and 5,703±410 μM CH_4, respectively) indicating that yeast extract is not essential for methanogenic growth. Observed methane concentrations were higher in incubations amended with DMA (10,115±836 μM CH_4) and TMA (9,524±3,626 μM CH_4, with a wide range of 5,361-11,993 μM) on average more than the MMA controls, consistent with what has been observed for other methylotrophic methanogens (40). Incubations amended with 10 mM methanol (MeOH) did not produce methane after 47 days of incubation at 70 ˚C. Due to its use by sulfate reducing organisms as an electron

donor (41), 10 mM lactate (LAC) was tested, as well as 10 mM MMA with 10 mM LAC, but none of these incubations produced methane. Production of methane has not been observed in any attempted transfers where only hydrogen (99.9999% purity) was present in the headspace, or hydrogen with MMA was added (data not shown).

The enrichment grew optimally at both 64 and 70 ˚C with relative amounts of methane produced at 5,304±451 μM and 5,202±606 μM, respectively. This is in contrast to the predicted optimal growth temperature of 74.4˚C deduced from the *Ca.* M. hypatiae MAG via Tome (42). This is lower than the observed range of growth and optimum temperatures for type strains of non-methanogenic Archaeoglobus which have been demonstrated to grow between 50 and 95 ˚C with optimal temperatures between 75-83 ˚C in organisms sourced predominantly from deep sea vent environments (30). No methane production was detected at temperatures 77 ˚C or above or lower than 64 ˚C after 47 days of incubation (Dataset S4).

Genomic and Transcriptomic Basis for Methanogenesis

The assembled metagenome obtained at the end of the SIT experiment was used to align a total of 23,376,154 million metatranscriptome mRNA reads obtained from six replicates harvested in the exponential growth phase and to create a detailed reconstruction of the metabolism of *Ca.* M. hypatiae (Fig. 3AB, 5, Dataset S5). A total of 22,891,651 reads, *i.e.,* 97.8% of all recovered reads, were recruited to the *Ca.* M. hypatiae MAG. Only 2.1% of the total mRNA reads (484,503) were aligned with other co-enriched organisms. Among these, only 13 genes across four MAGs were expressed above 200 RPKM and just five genes exceeded >1,000 RPKM. Notably, genes required for the conversion of methylamine to methane were among the top 2% of highest expressed genes transcribed by *Ca.* M. hypatiae, including genes encoding the MCR complex (*mcrAGCDB*; 15,976 RPKM), monomethylamine methyltransferase (*mtmB*; 884-9,884 RPKM), dimethylamine corrinoid (*mtbC*; 3,677 RPKM), and methanol:coenzyme M methyltransferase (*mtaA*; 12,577 RPKM) (Fig. 5). Seven copies of substrate-specific methyltransferases for MMA (*mtmB*; 3 copies), DMA (*mtbB*; 2 copies), and TMA (*mttB*; 2 copies) were present in the genome, but methanol methyltransferase (*mtaB*) was not identified. These genes were differentially expressed with one copy for each type of methylamine expressed above 3,200 RPKM. In addition to *mtbC*, two gene copies of the trimethylamine corrinoid protein (*mttC*) were found in the genome but their expression was relatively low (<460 RPKM average). Monomethylamine corrinoid (*mtmC*) or methanol corrinoid (*mtaC*) proteins were not identified in *Ca.* M. hypatiae. Additionally, genes were expressed for pyrrolysine synthesis (*pylBCD*; 819, 343, 37 RPKM) and the methyltransferase corrinoid activation protein (*ramA*; 1,076 RPKM), both of which support methylamine methyltransferases in methylotrophic methanogenesis (43, 44). The absence of *mtmC* and the high expression levels of *mtbC* (3,677 RPKM) and *mtaA* (12,577 RPKM) suggests that they are responsible for the transfer of a methyl group from monomethylamine to coenzyme M (CoM) after it has been transferred by a substrate-specific methyltransferase (*mtmB*). Consistent with the observed methane production from DMA and TMA, *Ca.* M. hypatiae can use these methylamines and expressed the corresponding genes (*mtbB*, *mttB*) at comparatively high levels (JOOIALLP_01813 *mtbB* 3,249 RPKM; JOOIALLP_01787 *mttB* 5,324 RPKM; Fig. 4B, 5). It is worth noting that the expression of these genes was detected despite the culture not having been previously exposed to DMA or TMA at the time of the transcriptomics experiment. We hypothesize that *Ca.* M. hypatiae could employ one of two strategies: it either (i) constitutively expresses all substrate-specific methyltransferases and corrinoid proteins as a precautionary measure to accommodate substrates potentially encountered *in situ*, or (ii) *Ca.* M. hypatiae transcriptionally co-regulates the genes responsible for these functions.

261 *Ca.* M. hypatiae expressed the methyl-branch of the Wood-Ljungdahl pathway (WLP) and the acetyl-
262 CoA decarbonylase/synthase complex (Cdh, *cdhABCDE*), which is consistent with genes observed and
263 shown to be expressed in sulfate-reducing Archaeoglobi genomes (41). This includes two paralogous copies
264 of 5,10-methylenetetrahydromethanopterin reductase (*mer*) which might function as a traditional Mer,
265 considering that these genes are also members of the large luciferase-like monooxygenase family
266 (pfam00296)(35). The expression of genes in the WLP varied. Methylenetetrahydromethanopterin
267 dehydrogenase (*mtd*), methenyltetrahydromethanopterin cyclohydrolase (*mch*), formylmethanofuran-
268 tetrahydromethanopterin N-formyltransferase (*ftr*), formylmethanofuran dehydrogenase (*fwdABC*), and
269 one copy of the *mer* homologs were expressed at comparatively high levels (456-2,763 RPKM), while
270 FwdDEFG and the other *mer* copy were only minimally expressed (<180 RPKM). The high expression of
271 the Cdh complex (*cdhACDE*; 3,063±362, *cdhB* 677 RPKM average across subunits) suggests that *Ca.* M.
272 hypatiae is capable of autotrophically fixing CO_2 to acetyl-CoA as has been shown for other *Archaeoglobus*
273 species (45). Acetyl-CoA could also be derived from the degradation of fatty acids present in yeast extract
274 through the process of beta-oxidation. Enzymes involved in this pathway were expressed at moderate to
275 high levels during growth (340-3,864 RPKM). Pyruvate synthase (Por) was highly expressed providing a
276 way for acetyl-CoA to be converted to pyruvate and subsequently be fed into major biosynthetic pathways.
277 Specifically, *Ca.* M. hypatiae encodes pyruvate carboxylase (PycAB), an incomplete reductive
278 tricarboxylic acid cycle (rTCA), phosphoenolpyruvate synthase (Pps), most enzymes needed for
279 gluconeogenesis, and several enzymes associated with the pentose phosphate pathway in archaea, which
280 were all expressed at varying levels (Dataset S5). Together, these pathways provide *Ca.* M. hypatiae the
281 capacity to synthesize amino acids, carbohydrates, integral components of the cell wall, and vital sugars for
282 nucleic acids.
283 Several complexes related to energy conservation and electron transport were moderately to highly
284 expressed. *Ca.* M. hypatiae encodes a fused heterodisulfide reductase (*hdrDE*) that was highly expressed
285 (1,106±120 RPKM) in addition to a fused *hdrD/mvhD* and four copies of *hdrD* that were all expressed at
286 much lower levels (<500 RPKM). The differing levels of transcription suggest the membrane-bound HdrDE
287 is responsible for the regeneration of coenzymes M and B through the reduction of heterodisulfide (CoM-
288 S-S-CoB). Additionally, the absence of HdrB, which contains the active site for disulfide reduction,
289 eliminates the possibility that disulfide reduction could occur via a HdrABC complex (46). A unique gene
290 cluster was identified containing F_{420}-non-reducing hydrogenase (MvhAGD), two HdrA copies and a
291 QmoC fused to a HdrC. One HdrA copy (JOOIALLP_01710) was predicted by DiSCo analysis as a
292 quinone-modifying oxidoreductase (QmoB), a protein related to the HdrA of methanogens (47, 48). This
293 cluster was expressed at high levels (995-2,431 RPKM average), suggesting its importance for electron
294 transfer in *Ca.* M. hypatiae. We hypothesize these subunits are associating together *in vivo* to bifurcate
295 electrons from hydrogen (H_2) to reduce both menaquinone (MQ) and ferredoxin (Fd_{ox}), as proposed recently
296 (35, 49). Lastly, *Ca.* M. hypatiae moderately expressed a membrane-bound $F_{420}H_2$:quinone oxidoreductase
297 (Fqo) complex (88-280 RPKM across subunits) and a V-type ATP synthase (24-442 RPKM across
298 subunits).
299 The reductant required for reducing the CoM-S-S-CoB made during conversion of methylated
300 substrates to methane during methylotrophic methanogenesis can originate from two possible routes. The
301 first possibility would rely on sourcing electrons from hydrogen, which could be oxidized by the Mvh-
302 Qmo-Hdr complex coupled to menaquinone reduction. H_2 may be produced through the activity of a group
303 3b [NiFe]-sulfhydrogenase (HydABDG), which was the highest expressed hydrogenase complex with an
304 average RPKM of 4,421 across subunits (50, 51). To evolve hydrogen via HydABDG, reducing power, via

NADPH, could be supplied by sulfide dehydrogenase (SudAB; Sud A, 1,088 RPKM; SudB, 495 RPKM). Alternatively, NADPH could instead be provided to biosynthesis pathways and therefore be decoupled from methanogenic metabolism. H_2 could also potentially be sourced from fermentative bacteria in the enrichment culture, however, the low number of hydrogenases encoded by co-enriched organisms were only very lowly expressed at the time of sampling for metatranscriptomics (<51 RPKM). At this point, the source of H_2 *Ca.* M. hypatiae uses remains uncertain, as no H_2 was added to the headspace. Second, in a hydrogen-independent electron transport system, reduced F_{420} and ferredoxin could be produced through the dismutation of methylated substrate to CO_2 through the WLP. Reduced F_{420} could be oxidized by the Fqo complex and contribute to a reduced menaquinone pool that could be used by the fused HdrDE complex to reduce CoM-S-S-CoB. Reduced ferredoxin could be oxidized at a soluble FqoF to reduce F_{420} or at an Fqo complex lacking FqoF to reduce menaquinone (52, 53). Based on the low expression levels of the Fqo complex (171±67 RPKM) and the absence of F_{420}-reducing hydrogenase (*frh*) from the genome, it is not likely the WLP runs in the reductive direction as a source of reduced F_{420} would be required. Resolving the exact configuration of the electron transport system encoded by *Ca.* M. hypatiae will require biochemical confirmation in future investigations.

Importantly, genes necessary for dissimilatory sulfate reduction typically observed in sulfate-reducing members of the Archaeoglobi, including dissimilatory sulfite reductase (*dsrAB*), sulfate adenylyltransferase (*sat*), and adenylylsulfate reductase (*aprAB*), were neither identified in the genome of *Ca.* M. hypatiae nor in the unbinned fraction of the metagenome. They were also absent from the comparatively incomplete MAG of *Ca.* M. nevadensis GBS (35). However, *Ca.* M. hypatiae encodes subunits *dsrMK* and *dsrOP* of the Dsr complex in addition to *dsrC*. This complex is strictly conserved in sulfate-reducing organisms (54) where it mediates electron transfer from the periplasm to the cytoplasm reducing the disulfide bond found in DsrC cysteines (55). The expression of the Dsr complex and *dsrC* was low (450±63 RPKM) during growth on monomethylamine suggesting it is not vital to the metabolism of *Ca.* M. hypatiae. The presence of the Dsr complex, DsrC, and subunits QmoC and QmoB in the genome may be explained as evolutionary remnants from ancestral Archaeoglobi, which initially grew as sulfate-reducing organisms but later transitioned to a methanogenic lifestyle (7, 8). This raises the question whether intermediate of this process, Archaeoglobi capable of both methanogenesis and sulfate-reduction (and possible anaerobic oxidation of methane), still exist today.

Collectively, the metagenomic and transcriptomic data confirmed that *Ca.* M. hypatiae is not only the sole archaeon but the sole methanogen in our culture. The metabolic reconstruction and metatranscriptomics results are consistent with methylotrophic methanogenesis from methylamines. The absence of genes required for sulfate reduction eliminates the possibility for this metabolism in *Ca.* M. hypatiae. A unique gene cluster (Mvh-Qmo-Hdr) potentially involved in energy conservation was expressed, however future studies will be required to test how *Ca.* M. hypatiae internally cycles electrons for methanogenesis and if it sources H_2, or other reductants, from the medium or co-enriched bacteria.

Distribution of *Ca.* Methanoglobus Across Geothermal Features in YNP

16S rRNA and *mcrA* gene amplicon sequence data generated in a recent microbial diversity survey of 100 geothermal features in YNP (33) were used to analyze the distribution of Archaeoglobi related to *Ca.* M. hypatiae (SI Appendix, Fig. S5). 16S rRNA gene amplicons closely related to *Ca.* M. hypatiae (96.7-100% sequence identity) were found in seven DNA samples from six hot springs (pH 5.1-9.35, 31-78 ºC) in addition to hot spring LCB024 (the source of this culture) at relative abundances ranging from 0.02-0.22%. In addition, *mcrA* gene ASVs affiliated with Archaeoglobi were PCR-amplified from 53 DNA

samples. These were collected from microbial mats or sediments originating from 36 geothermal features distributed across various thermal regions within YNP by Lynes, Krukenberg *et al.* (33). Archaeoglobi-related *mcrA* genes were found in geothermal features with a pH range of 2.61 to 9.32 and a temperature range of 18.4 ºC to 93.8 ºC. Collectively, our results and the studies by Wang *et al*. and Buessecker *et al*., who reported that Mcr-encoding Archaeoglobi are present (35) and transcriptionally active in hot spring mesocosms (34), demonstrate the previously overlooked role Archaeoglobi might play in the anaerobic carbon cycle of geothermal environments.

Conclusion

In summary, the cultivation of *Ca.* Methanoglobus hypatiae LCB24 provides direct experimental evidence that members of the Archaeoglobi are methanogens. *Ca.* M. hypatiae can use MMA, DMA, and TMA as methanogenic substrates and grows optimally at 64-70 ºC, as evidenced by metagenomics, metatranscriptomics, and isotope tracing experiments. Metagenomic sequencing and phylogenomic analysis confirmed the close relationship of *Ca.* M. hypatiae to other Mcr-encoding Archaeoglobi and the relatedness of its *mcrA* to MAGs of the TACK superphylum, some of which have recently been showed to also be methanogens (56, 57). Together, this supports the idea that the capacity for methanogenesis is deeply rooted in the archaea and possibly dates to the last common ancestor of archaea (1, 3, 7, 8, 58). The wide distribution of Archaeoglobi-affiliated *mcrA* gene sequences and *Ca.* M. hypatiae-related 16S rRNA gene sequences in geothermal features across YNP suggests that members of this lineage play a hitherto unaccounted-for role in anaerobic carbon cycling in these extreme ecosystems. Future studies of *Ca.* M. hypatiae and other methanogens will provide valuable insights into the evolution of methane metabolism and the significance of these archaea in biogeochemical cycles across geothermal and other environments.

Materials and Methods

All chemicals used in this study were sourced from Sigma Aldrich unless otherwise specified.

Sample Collection, Enrichment, and Cultivation

In November 2021, a slurry of sediment and water (1:9) was collected from an unnamed hot spring in the Lower Culex Basin of Yellowstone National Park (YNP), WY, USA. In our previous survey of Mcr-encoding archaea in YNP (33), this hot spring was given the identifier LCB024 (44.573294, -110.795388; pH 7.8, 67 ˚C). A mixture of surface sediment (~1-2 cm deep) and hot spring water was collected into a glass bottle and sealed headspace-free with a thick butyl rubber stopper. Collected material was transported back to the lab and stored at room temperature. Using this material as inoculum, 30 mL enrichments were established in February 2022 in 60 mL serum bottles. Material was homogenized by mixing and was then diluted 1:10 (v/v) with anoxic medium in an anoxic glove box ($N_2/CO_2/H_2$; 90/5/5%).

Medium was prepared anoxically as described previously (59) and contained a base of (per liter): KH_2PO_4, 0.5 g; $MgSO_4 \cdot 7H_2O$, 0.4 g; NaCl, 0.5 g; NH_4Cl, 0.4 g; $CaCl_2 \cdot 2H_2O$, 0.05 g; HEPES, 2.38 g; yeast extract, 0.1 g; and 0.002% (w/v) $(NH_4)_2Fe(SO_4)_2 \cdot 6H_2O$, 5 mM $NaHCO_3$, 1 mL trace element solution SL-10, 1 mL Selenite-Tungstate solution, 1 mL CCM vitamins (60), 0.0005% (w/v) resazurin, 10 mg of coenzyme-M, 2 mg sodium dithionite, 1 mM dithiothreitol, 1 mM $Na_2S \cdot 9H_2O$, with pH adjusted to 7.8. Serum bottles were sealed with butyl rubber stoppers and aluminum crimps before the headspace was exchanged with N_2 (99.999%) for 5 minutes and set to a 200 kPa N_2 atmosphere. Monomethylamine (MMA) was added from a filter-sterilized methylamine-hydrochloride anoxic stock solution to a final concentration of 10 mM. The bacterial antibiotics streptomycin (50 mg/L; inhibitor of protein synthesis)

and vancomycin (50 mg/L; inhibitor of peptidoglycan synthesis) were added from filter-sterilized anoxic stock solutions. The enrichments were incubated at 70 ˚C in the dark without shaking. Cultures were maintained by regular transfer of 10% v/v into fresh media, which contained MMA and antibiotics. A sediment-free culture was obtained after the third transfer after which it was transferred at 10% v/v to 50 mL in 125 mL serum bottles.

Stable Isotope Tracing

The conversion of ^{13}C- or D_3-MMA ($^{13}CH_3$-NH_2, CD_3-NH_2) to $^{13}CH_4$ or CD_3H was tracked by incubating active enrichment cultures in the presence of 20% labeled substrate (98%; Cambridge Isotope Laboratories). Incubations were carried out in 30 mL culture volumes in 60 mL serum bottles with 8% v/v inoculum, 50 mg/L streptomycin, 50 mg/L vancomycin, 10 mM MMA, and N_2 gas (99.999%) incubated in anoxic media (pH 7.8, 70 ˚C) in six replicates (SI Appendix, Fig. S3). Duplicate control incubations included (i) ^{12}C-MMA and (ii) inoculum without MMA. Triplicate control incubations were performed with (iii) ^{12}C-MMA plus 10 mM bromoethanesulfonate (BES) added in mid-exponential phase (day 33) to inhibit methanogenesis and (iv) 10 mM BES added at time of inoculation (day 0) without substrate. Headspace samples were collected throughout the experiment as described above and analyzed using a Shimadzu QP2020 NX GCMS equipped with a GS-CarbonPLOT column (30 m × 0.35 mm; 1.5 µm film thickness; Agilent) and operated in Selected Ion Monitoring mode. The instrument was operated using the method described in Ai et al., 2013 (61) with helium as a carrier gas. Peak areas corresponding to m/z ratios of 16 for $^{12}CH_4$, 17 for $^{13}CH_4$, and 19 for CD_3H were used for quantification.

Metagenomic Sequencing, Assembly, and Annotation

Two metagenomes were obtained over the course of this study. A 42 mL aliquot of the fourth transfer of the enrichment (Fig. 1 T4-MG) was filtered onto a 0.22 µm filter, transferred to a lysing matrix E tube, and DNA extracted immediately following filtration. Genomic DNA was extracted using the FastDNA Spin Kit for Soil (MP Biomedicals, Irvine, CA) following the manufacturer's guidelines.

A second metagenome was recovered from one of the six culture replicates grown in the presence of CD_3-NH_2 and used for recruiting transcriptomic reads from the other replicates (Fig. 1 SIT-MG). A 60 mL syringe flushed with N_2 gas was used to transfer 30 mL of culture to a sterilized oak ridge tube. Cells were harvested through centrifugation for 30 minutes at 10,000 rpm at 4 ˚C. The supernatant was removed, and DNA extracted from the pellet using the FastDNA Spin Kit for Soil (MP Biomedicals, Irvine, CA) following the manufacturer's guidelines.

Genomic DNA for both metagenomes was shipped to SeqCenter (Pittsburgh, PA) and sample libraries were prepared using the Illumina DNA Prep kit and 10bp unique dual indices (UDI). The first metagenome (T4-MG) was sequenced on an Illumina NextSeq 2000 and the second (SIT-MG) sequenced on an Illumina NovaSeq 6000, each producing 2x151bp reads. Demultiplexing, quality control, and adapter trimming was performed with bcl-convert v3.9.3. Quality of the reads were evaluated with FastQC before quality, linker and adapter trimming, artifact and common contaminate removal, and error correction were performed with the rqcfilter2 pipeline (maxn=3, maq=10, trimq=15 (first dataset), trimq=20 (second dataset)) and bbcms (mincount=2, hcf=0.6). Resulting reads were assembled with SPAdes v3.15.13 (Nurk, 2017) (-k 33,55,77,99,127 --meta –only-assembler) and coverage was determined with bbmap (ambiguous=random). Combined assemblies were performed with the trimmed and error corrected reads and the same assembly parameters, or with the raw reads but excluding the –only-assembler option. Annotation of the assembled sequences was performed with Prokka v1.14.16 (62). Assembled scaffolds

≥2000 bp were binned using Maxbin v2.2.7 (63), Metabat v2.12.1 (with and without coverage) (64), Concoct v1.0.0 (65), Autometa v1 (bacterial and archaeal modes with the machine learning step) (66), followed by bin refinement with DAS_Tool v1.1.6 (67), as previously described (68). Bin completeness and redundancy were assessed with CheckM v1.2.2 (69).

RNA Extraction, Sequencing, and Transcriptomic Processing

Total RNA was extracted for transcriptomics from four of the six replicates of Archaeoglobus cultivated in the presence of labeled substrate ($^{13}CH_3$-NH_2 or CD_3-NH_2) for a total of eight replicates. Each replicate culture in the exponential growth phase (day 32) was moved from the 70 ˚C incubator to an ice bath placed at -20 ˚C for 40 minutes to stop cellular activity. A 60 mL syringe flushed with N_2 gas was used to transfer 30 mL of culture to a sterilized oak ridge tube and kept on ice. Cells were harvested through centrifugation for 30 minutes at 10,000 rpm at 4 ˚C. The supernatant was removed, and the pellet transferred to a lysing matrix E tube (MP Biomedicals, Irvine, CA) to which 600 µL of RNA lysis buffer was added. Samples were homogenized in a MP Bioscience FastPrep instrument for 40 seconds at a speed setting of 6.0 m/s followed by centrifugation for 15 minutes at 14,000 rpm. RNA was extracted using the Quick-RNA miniprep kit (Zymo Research, Irvine, CA) including a DNAse treatment step and eluted in 50 µL of RNAse free water. Centrifugation steps were performed at 15,000 rpm and the final spin for elution at 10,000 rpm. Of the eight replicates extracted, six measured >50 ng/µL (3x $^{13}CH_3$-NH_2 and 3x CD_3-NH_2) and were sent for transcriptomic sequencing at SeqCenter (Pittsburgh, PA). Samples were DNAse treated with Invitrogen DNAse (RNAse free). Library preparation was performed using Illumina's Stranded Total RNA Prep Ligation with Ribo-Zero Plus kit and 10bp UDI. Sequencing was done on a NovaSeq 6000, producing paired end 151bp reads. Demultiplexing, quality control, and adapter trimming was performed with bcl-convert (v4.1.5). Read quality was further evaluated with FastQC v0.11.9 (70) before quality trimming and artifact, rRNA, and common contaminant removal with the rqcfilter2 pipeline (trimq=28, maxns=3, maq=20), and error correction with bbcms (mincount=2, hcf=0.6) from the BBTools suite v38.94 (71). BBMap: a fast accurate, splice-aware aligner. https://sourceforge.net/projects/bbmap). Additional rRNA gene reads were detected and removed with Ribodetector v0.2.7 (72) and any remaining rRNA gene reads were finally removed with bbmap, using rRNA genes recovered from the metagenomes (see below) as references. The resulting mRNA reads were mapped against annotated genes from the paired metagenomes with bbmap (ambig=random).

Data Availability

All metagenomic, metatranscriptomic, and amplicon data discussed in this manuscript are available under NCBI BioProject ID PRJNA1014417. McrA gene amplicon data from YNP hot springs discussed in this manuscript has been previously published (Lynes et al., 2023) and is available under NCBI under BioProject PRJNA859922.

Acknowledgements

This study was funded through a NASA Exobiology program award (80NSSC19K1633) to R.H. We thank the US National Park Service for permitting work in YNP under permit number YELL-SCI-8010. We thank George Schaible (MSU) for help with SEM imaging, Dr. Viola Krukenberg (MSU) for initial FISH methodology development, Sylvia Nupp, Dr. Andrew Montgomery, and Paige Schlegel (all MSU) for assistance with field sampling, Dr. Christopher Lemon (MSU) for allowing use of his cooling centrifuge, and Dr. Marike Palmer (UN Las Vegas) for discussing naming of this archaeon.

References

1. J. M. Wolfe, G. P. Fournier, Horizontal gene transfer constrains the timing of methanogen evolution. *Nat Ecol Evol* **2**, 897-903 (2018).
2. D. Y. Sorokin *et al.*, Discovery of extremely halophilic, methyl-reducing euryarchaea provides insights into the evolutionary origin of methanogenesis. *Nat Microbiol* **2**, 17081 (2017).
3. W. F. Martin, F. L. Sousa, Early Microbial Evolution: The Age of Anaerobes. *Cold Spring Harb Perspect Biol* **8**, a018127 (2015).
4. B. Sauterey, B. Charnay, A. Affholder, S. Mazevet, R. Ferrière, Co-evolution of primitive methane-cycling ecosystems and early Earth's atmosphere and climate. *Nature Communications* **11**, 2705 (2020).
5. Y. Ueno, K. Yamada, N. Yoshida, S. Maruyama, Y. Isozaki, Evidence from fluid inclusions for microbial methanogenesis in the early Archaean era. *Nature* **440**, 516-519 (2006).
6. A. Spang, T. J. G. Ettema, Archaeal evolution: The methanogenic roots of Archaea. *Nature Microbiology* **2**, 17109 (2017).
7. P. S. Adam, G. E. Kolyfetis, T. L. V. Bornemann, C. E. Vorgias, A. J. Probst, Genomic remnants of ancestral methanogenesis and hydrogenotrophy in Archaea drive anaerobic carbon cycling. *Science Advances* **8**, eabm9651 (2022).
8. Y. Wang *et al.*, A methylotrophic origin of methanogenesis and early divergence of anaerobic multicarbon alkane metabolism. *Science Advances* **7**, eabj1453 (2021).
9. K.-U. Hinrichs, Microbial fixation of methane carbon at 2.7 Ga: Was an anaerobic mechanism possible? *Geochemistry, Geophysics, Geosystems* **3**, 1-10 (2002).
10. M. Saunois *et al.*, The Global Methane Budget 2000–2017. *Earth Syst. Sci. Data* **12**, 1561-1623 (2020).
11. J. A. Rosentreter *et al.*, Half of global methane emissions come from highly variable aquatic ecosystem sources. *Nature Geoscience* **14**, 225-230 (2021).
12. P. S. Garcia, S. Gribaldo, G. Borrel, Diversity and Evolution of Methane-Related Pathways in Archaea. *Annual Review of Microbiology* **76**, null (2022).
13. J. G. Ferry, K. A. Kastead, "Methanogenesis" in Archaea. (2007), https://doi.org/10.1128/9781555815516.ch13, pp. 288-314.
14. R. Conrad, The global methane cycle: recent advances in understanding the microbial processes involved. *Environ Microbiol Rep* **1**, 285-292 (2009).
15. S. Scheller, M. Goenrich, R. Boecher, R. K. Thauer, B. Jaun, The key nickel enzyme of methanogenesis catalyses the anaerobic oxidation of methane. *Nature* **465**, 606-608 (2010).
16. R. K. Thauer, Methyl (Alkyl)-Coenzyme M Reductases: Nickel F-430-Containing Enzymes Involved in Anaerobic Methane Formation and in Anaerobic Oxidation of Methane or of Short Chain Alkanes. *Biochemistry* **58**, 5198-5220 (2019).
17. P. N. Evans *et al.*, An evolving view of methane metabolism in the Archaea. *Nat Rev Microbiol* **17**, 219-232 (2019).
18. R. K. Thauer, A. K. Kaster, H. Seedorf, W. Buckel, R. Hedderich, Methanogenic archaea: ecologically relevant differences in energy conservation. *Nat Rev Microbiol* **6**, 579-591 (2008).
19. B. J. Baker *et al.*, Diversity, ecology and evolution of Archaea. *Nat Microbiol* **5**, 887-900 (2020).

20. C. P. Bueno de Mesquita, D. Wu, S. G. Tringe, Methyl-Based Methanogenesis: an Ecological and Genomic Review. *Microbiol Mol Biol Rev* **87**, e0002422 (2023).
21. A. Söllinger, T. Urich, Methylotrophic methanogens everywhere — physiology and ecology of novel players in global methane cycling. *Biochemical Society Transactions* **47**, 1895-1907 (2019).
22. M. K. Nobu, T. Narihiro, K. Kuroda, R. Mei, W. T. Liu, Chasing the elusive Euryarchaeota class WSA2: genomes reveal a uniquely fastidious methyl-reducing methanogen. *ISME J* **10**, 2478-2487 (2016).
23. I. Vanwonterghem *et al.*, Methylotrophic methanogenesis discovered in the archaeal phylum Verstraetearchaeota. *Nat Microbiol* **1**, 16170 (2016).
24. L. J. McKay *et al.*, Co-occurring genomic capacity for anaerobic methane and dissimilatory sulfur metabolisms discovered in the Korarchaeota. *Nat Microbiol* **4**, 614-622 (2019).
25. Y. Wang, G. Wegener, J. Hou, F. Wang, X. Xiao, Expanding anaerobic alkane metabolism in the domain of Archaea. *Nat Microbiol* **4**, 595-602 (2019).
26. P. N. Evans *et al.*, Methane metabolism in the archaeal phylum Bathyarchaeota revealed by genome-centric metagenomics. *Science* **350** (2015).
27. B. A. Berghuis *et al.*, Hydrogenotrophic methanogenesis in archaeal phylum Verstraetearchaeota reveals the shared ancestry of all methanogens. *Proc Natl Acad Sci U S A* **116**, 5037-5044 (2019).
28. Y. F. Liu *et al.*, Genomic and Transcriptomic Evidence Supports Methane Metabolism in Archaeoglobi. *mSystems* **5** (2020).
29. K. O. Stetter, G. Lauerer, M. Thomm, A. Neuner, Isolation of Extremely Thermophilic Sulfate Reducers: Evidence for a Novel Branch of Archaebacteria. *Science* **236**, 822-824 (1987).
30. G. Slobodkina *et al.*, Physiological and Genomic Characterization of a Hyperthermophilic Archaeon Archaeoglobus neptunius sp. nov. Isolated From a Deep-Sea Hydrothermal Vent Warrants the Reclassification of the Genus Archaeoglobus. *Front Microbiol* **12**, 679245 (2021).
31. J. A. Boyd *et al.*, Divergent methyl-coenzyme M reductase genes in a deep-subseafloor Archaeoglobi. *ISME J* **13**, 1269-1279 (2019).
32. Z. S. Hua *et al.*, Insights into the ecological roles and evolution of methyl-coenzyme M reductase-containing hot spring Archaea. *Nat Commun* **10**, 4574 (2019).
33. M. M. Lynes *et al.*, Diversity and function of methyl-coenzyme M reductase-encoding archaea in Yellowstone hot springs revealed by metagenomics and mesocosm experiments. *ISME Communications* **3**, 22 (2023).
34. J. Wang *et al.*, Evidence for nontraditional mcr-containing archaea contributing to biological methanogenesis in geothermal springs. *Science Advances* **9**, eadg6004 (2023).
35. S. Buessecker *et al.*, Mcr-dependent methanogenesis in Archaeoglobaceae enriched from a terrestrial hot spring. *The ISME Journal* 10.1038/s41396-023-01472-3 (2023).
36. D. A. Stahl, Development and application of nucleic acid probes in bacterial systematics. *Nucleic Acid Techniques in Bacterial Systematics*, 205-248 (1991).
37. K. O. Stetter, Archaeoglobus fulgidus gen. nov., sp. nov.: a new taxon of extremely thermophilic archaebacteria. *Syst. Appl. Microbiol.* **10**, 172-173 (1988).
38. H. Huber, H. Jannasch, R. Rachel, T. Fuchs, K. O. Stetter, Archaeoglobus veneficus sp. nov., a Novel Facultative Chemolithoautotrophic Hyperthermophilic Sulfite Reducer,

Isolated from Abyssal Black Smokers. *Systematic and Applied Microbiology* **20**, 374-380 (1997).

39. K. Mori, A. Maruyama, T. Urabe, K.-i. Suzuki, S. Hanada, Archaeoglobus infectus sp. nov., a novel thermophilic, chemolithoheterotrophic archaeon isolated from a deep-sea rock collected at Suiyo Seamount, Izu-Bonin Arc, western Pacific Ocean. *International Journal of Systematic and Evolutionary Microbiology* **58**, 810-816 (2008).
40. A. J. Watkins, E. G. Roussel, G. Webster, R. J. Parkes, H. Sass, Choline and N,N-dimethylethanolamine as direct substrates for methanogens. *Appl Environ Microbiol* **78**, 8298-8303 (2012).
41. W. P. Hocking, R. Stokke, I. Roalkvam, I. H. Steen, Identification of key components in the energy metabolism of the hyperthermophilic sulfate-reducing archaeon Archaeoglobus fulgidus by transcriptome analyses. *Frontiers in microbiology* **5**, 95 (2014).
42. G. Li, K. S. Rabe, J. Nielsen, M. K. Engqvist, Machine learning applied to predicting microorganism growth temperatures and enzyme catalytic optima. *ACS synthetic biology* **8**, 1411-1420 (2019).
43. A. Mahapatra *et al.*, Characterization of a Methanosarcina acetivorans mutant unable to translate UAG as pyrrolysine. *Mol Microbiol* **59**, 56-66 (2006).
44. T. Ferguson, J. A. Soares, T. Lienard, G. Gottschalk, J. A. Krzycki, RamA, a protein required for reductive activation of corrinoid-dependent methylamine methyltransferase reactions in methanogenic archaea. *J Biol Chem* **284**, 2285-2295 (2009).
45. S. Estelmann *et al.*, Carbon dioxide fixation in 'Archaeoglobus lithotrophicus': are there multiple autotrophic pathways? *FEMS microbiology letters* **319**, 65-72 (2011).
46. J. G. Ferry, How to make a living by exhaling methane. *Annu Rev Microbiol* **64**, 453-473 (2010).
47. N. A. Chernyh *et al.*, Dissimilatory sulfate reduction in the archaeon 'Candidatus Vulcanisaeta moutnovskia' sheds light on the evolution of sulfur metabolism. *Nat Microbiol* **5**, 1428-1438 (2020).
48. S. Neukirchen, F. L. Sousa, DiSCo: a sequence-based type-specific predictor of Dsr-dependent dissimilatory sulphur metabolism in microbial data. *Microbial Genomics* **7** (2021).
49. A. R. Ramos, K. L. Keller, J. D. Wall, I. A. C. Pereira, The membrane QmoABC complex interacts directly with the dissimilatory adenosine 5′ -phosphosulfate reductase in sulfate reducing bacteria. *Frontiers in microbiology* **3**, 137 (2012).
50. M. W. W. Adams, The metabolism of hydrogen by extremely thermophilic, sulfur-dependent bacteria. *FEMS Microbiology Reviews* **6**, 219-237 (1990).
51. K. Ma, R. N. Schicho, R. M. Kelly, M. Adams, Hydrogenase of the hyperthermophile Pyrococcus furiosus is an elemental sulfur reductase or sulfhydrogenase: evidence for a sulfur-reducing hydrogenase ancestor. *Proceedings of the National Academy of Sciences* **90**, 5341-5344 (1993).
52. W. P. Hocking, I. Roalkvam, C. Magnussen, R. Stokke, I. H. Steen, Assessment of the Carbon Monoxide Metabolism of the Hyperthermophilic Sulfate-Reducing Archaeon Archaeoglobus fulgidus VC-16 by Comparative Transcriptome Analyses. *Archaea* **2015**, 235384 (2015).
53. C. Welte, U. Deppenmeier, Membrane-bound electron transport in Methanosaeta thermophila. *J Bacteriol* **193**, 2868-2870 (2011).

54. I. A. Pereira, S. A. Haveman, G. Voordouw, Biochemical, genetic and genomic characterization of anaerobic electron transport pathways in sulphate-reducing delta-proteobacteria. *Sulphate-Reducing Bacteria: Environmental and Engineered Systems (LL, B. and WA, H., eds.), Cambridge University Press, Cambridge, UK* (2007).
55. F. Grein, I. A. Pereira, C. Dahl, Biochemical characterization of individual components of the Allochromatium vinosum DsrMKJOP transmembrane complex aids understanding of complex function in vivo. *Journal of bacteriology* **192**, 6369-6377 (2010).
56. K. Wu *et al.*, Isolation of a methyl-reducing methanogen outside the Euryarchaeota. (2023).
57. A. Kohtz *et al.*, Cultivation and visualization of a methanogen of the phylum Thermoproteota. (2023).
58. A. Spang, E. F. Caceres, T. J. G. Ettema, Genomic exploration of the diversity, ecology, and evolution of the archaeal domain of life. *Science* **357** (2017).
59. R. Laso-Perez, V. Krukenberg, F. Musat, G. Wegener, Establishing anaerobic hydrocarbon-degrading enrichment cultures of microorganisms under strictly anoxic conditions. *Nat Protoc* **13**, 1310-1330 (2018).
60. A. Brandis, R. K. Thauer, Growth of Desulfovibrio species on hydrogen and sulphate as sole energy source. *Microbiology* **126**, 249-252 (1981).
61. G. Ai, J. Zhu, X. Dong, T. Sun, Simultaneous characterization of methane and carbon dioxide produced by cultured methanogens using gas chromatography/isotope ratio mass spectrometry and gas chromatography/mass spectrometry. *Rapid Commun Mass Spectrom* **27**, 1935-1944 (2013).
62. T. Seemann, Prokka: rapid prokaryotic genome annotation. *Bioinformatics* **30**, 2068-2069 (2014).
63. Y.-W. Wu, Y.-H. Tang, S. G. Tringe, B. A. Simmons, S. W. Singer, MaxBin: an automated binning method to recover individual genomes from metagenomes using an expectation-maximization algorithm. *Microbiome* **2**, 26 (2014).
64. D. D. Kang, J. Froula, R. Egan, Z. Wang, MetaBAT, an efficient tool for accurately reconstructing single genomes from complex microbial communities. *PeerJ* **3**, e1165 (2015).
65. J. Alneberg *et al.*, Binning metagenomic contigs by coverage and composition. *Nat Methods* **11**, 1144-1146 (2014).
66. I. J. Miller *et al.*, Autometa: automated extraction of microbial genomes from individual shotgun metagenomes. *Nucleic Acids Res* **47**, e57 (2019).
67. C. M. K. Sieber *et al.*, Recovery of genomes from metagenomes via a dereplication, aggregation and scoring strategy. *Nat Microbiol* **3**, 836-843 (2018).
68. A. J. Kohtz, Z. J. Jay, M. M. Lynes, V. Krukenberg, R. Hatzenpichler, Culexarchaeia, a novel archaeal class of anaerobic generalists inhabiting geothermal environments. *ISME Communications* **2**, 86 (2022).
69. D. H. Parks, M. Imelfort, C. T. Skennerton, P. Hugenholtz, G. W. Tyson, CheckM: assessing the quality of microbial genomes recovered from isolates, single cells, and metagenomes. *Genome Res* **25**, 1043-1055 (2015).
70. S. Andrews, F. Krueger, A. Seconds-Pichon, F. Biggins, S. Wingett (2015) FastQC. A quality control tool for high throughput sequence data. Babraham Bioinformatics. Babraham Inst.

71. B. Bushnell (2014) BBMap: a fast, accurate, splice-aware aligner. (Lawrence Berkeley National Lab.(LBNL), Berkeley, CA (United States)).
72. Z.-L. Deng, P. C. Münch, R. Mreches, A. C. McHardy, Rapid and accurate identification of ribosomal RNA sequences via deep learning. *Nucleic acids research* **50**, e60-e60 (2022).

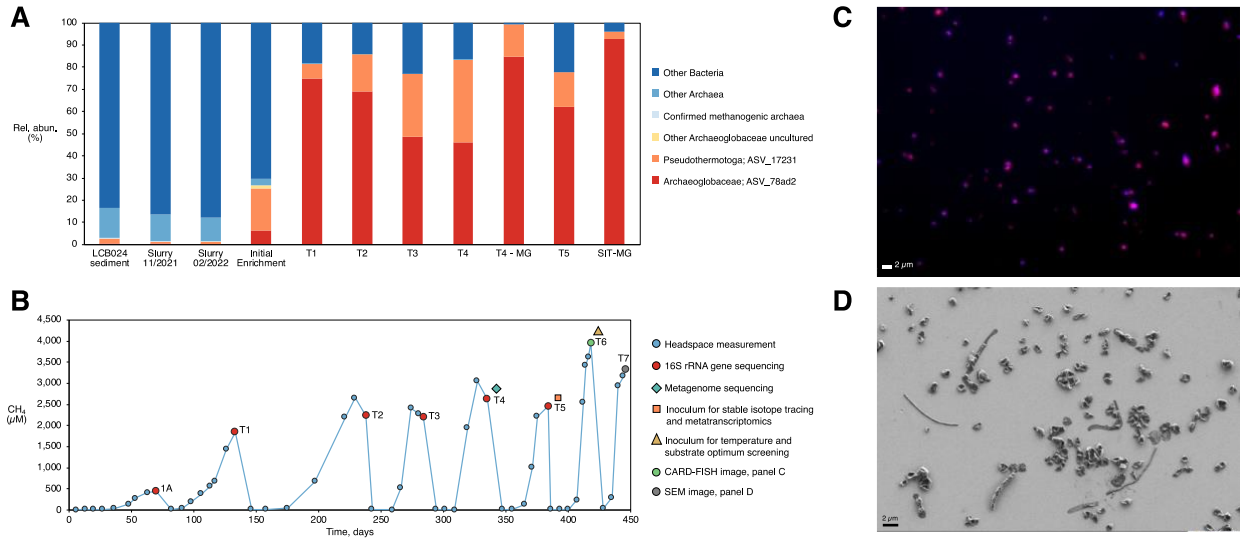

Fig. 1. Community composition and methane production of the methanogenic enrichment culture containing *Ca.* Methanoglobus hypatiae LCB24. *(A)* Relative abundance of 16S rRNA gene amplicons in the initial sediment from hot spring LCB024, the slurry collected in November 2021, slurry material used to initiate enrichments in February 2022, the initial enrichment, and five subsequent transfers (T1-T5) are shown. For comparison, the estimated relative abundance of two metagenomic samples (T4-MG and SIT-MG) is included. The metagenome recovered from a replicate from the stable isotope tracing experiment incubated in the presence of deuterated methylamine (SIT-MG) revealed *Ca.* M. hypatiae grew to 92.8% relative abundance during the experiment. The two most abundant ASVs across enrichment transfers are shown with other taxa collapsed. Other methanogenic archaea were not identified in the initial enrichment or in any subsequent transfers. Relative sequence abundance for all ASVs is reported in SI Appendix, Table S1. *(B)* Headspace methane produced over long-term cultivation. The time between transfers decreased while the average maximum concentration of methane increased over time. Culture 1A represents the initial enrichment. A history of methane measurements can be found in SI Appendix, Table S2. *(C)* Visualization of *Ca.* M. hypatiae cells at T6 labeled via CARD-FISH by the general archaea probe Arch915 (red). DAPI staining of cells is in blue. *(D)* Cell morphologies in enrichment culture LCB24 at T7 as observed by secondary electron microscopy.

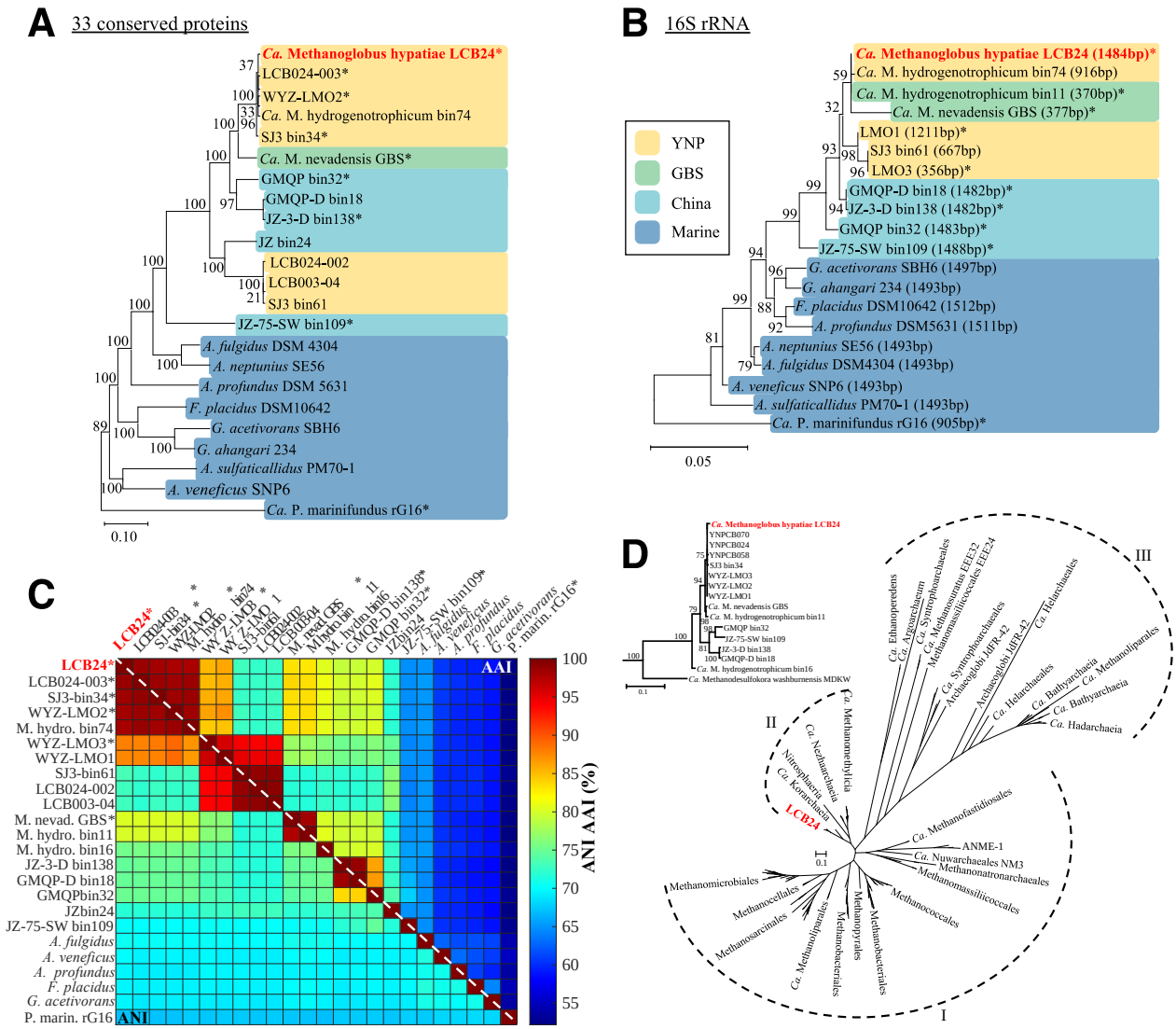

Fig. 2. Phylogenetic affiliation of *Ca.* M. hypatiae LCB24. *(A)* Maximum-likelihood tree, inferred with fasttree and WAG model (midpoint root), using a concatenated alignment of 33 conserved single copy proteins (list provided in SI Appendix, Table S4). References are colored by the habitat type from which sequences had been recovered: hot springs in Yellowstone National Park (YNP), yellow; Great Boiling Spring (GBS), green; hot springs in China, blue; marine hydrothermal vent systems, dark blue. *(B)* Maximum-likelihood tree inferred with fasttree using 16S rRNA genes with length in base pairs (bp). *(C)* ANI and AAI analysis of reference Archaeoglobales MAGs and genomes. Asterisks (*) indicate MAGs containing *mcrA*, apart from the MAG of *Ca.* M. hydrogenotrophicum bin74 which encodes a *mcrA* that is interrupted by a stop codon. AAI and ANI values are provided in SI Appendix, Fig. S1. *(D)* Maximum-likelihood tree, inferred with IQtree2 and the LG+C60+F+G model, from the amino acid alignment of McrA. Dashed lines indicate McrA/AcrA groups: (I) McrA from methanogens and ANME (MCR-type), (II) McrA from TACK lineages (MCR-type), (III) McrA-like from proposed and experimentally confirmed alkane oxidizing archaea (ACR-type). Insert shows MAGs closely related to *Ca.* M. hypatiae LCB24.

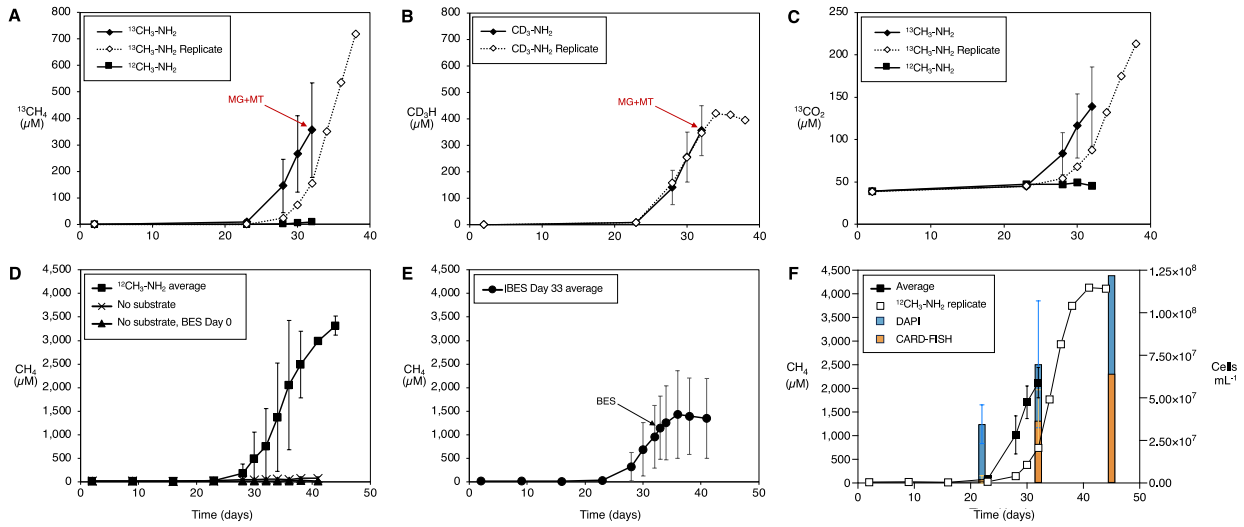

Fig. 3. Conversion of stable isotope labeled monomethylamine to methane by culture LCB24. *(A)* Production of $^{13}CH_4$ in cultures amended with $^{13}CH_3$-NH_2 vs. $^{12}CH_3$-NH_2 (6 replicates). *(B)* Production of CD_3H in cultures amended with CD_3-NH_2 (6 replicates). *(C)* Production of $^{13}CO_2$ in cultures amended with $^{13}CH_3$-NH_2 vs. $^{12}CH_3$-NH_2. For plots A and B, ten total replicates across treatments were sacrificed during mid-exponential phase for metagenomic or metatranscriptomic sequencing indicated by red arrows. $^{13}CH_4$, CD_3H, or $^{13}CO_2$ production for the replicate allowed to reach stationary phase is shown as a dashed line through open diamond symbols. *(D)* Production of $^{12}CH_4$ in cultures amended with ^{12}C-monomethylamine ($^{12}CH_3$-NH_2; 2 replicates). Cultures incubated without substrates (2 replicates) and those to which the inhibitor BES was added on day 0 (3 replicates) did not produce $^{12}CH_4$ over the course of the experiment. *(E)* Production of $^{12}CH_4$ in cultures amended with $^{12}CH_3$-NH_2 to which BES was added on day 33 of incubation (black arrow; 3 replicates). The average production of $^{12}CH_4$ leveled off and ceased after the introduction of BES, indicating methane generation by *Ca.* M. hypatiae is MCR-dependent. Error bars indicate standard deviation of biological replicates when applicable. Measurements of $^{12}CH_4$, $^{13}CH_4$, CD_3H, and $^{13}CO_2$ for all replicates and controls are reported in Dataset S2. $^{12}CH_4$ measurements for all controls and replicates are shown in SI Appendix, Fig. S4 and Dataset S3. *(F)* $^{12}CH_4$ production and fraction of *Ca.* M. hypatiae cells in biological replicates incubated with $^{13}CH_3$-NH_2. Relative abundance of cells was determined at three time points (day 22, 32, 45) based on the fraction of *Ca.* M. hypatiae specific CARD-FISH counts (orange) versus total counts of DAPI stained cells (blue). Error bars indicate the standard deviation for four biological replicates on days 22 and 32.

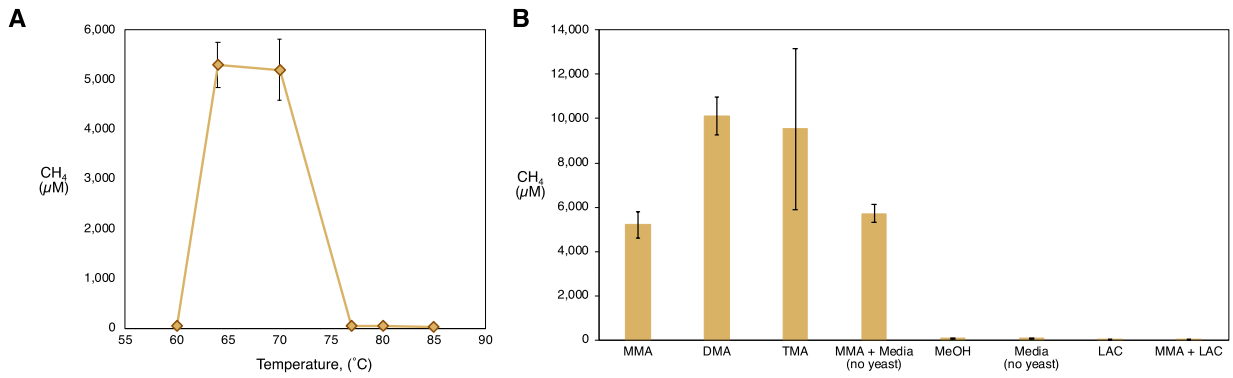

Fig. 4. Temperature and substrate range of culture LCB24. *(A)* Methane production from MMA was observed between 64-70 ˚C. *(B)* Substrate range. Methane production was observed for MMA, DMA, TMA, and in media prepared without yeast extract. LAC, lactate; MeOH, methanol. Both experiments performed in triplicate. All measurements can be found in Dataset S4.

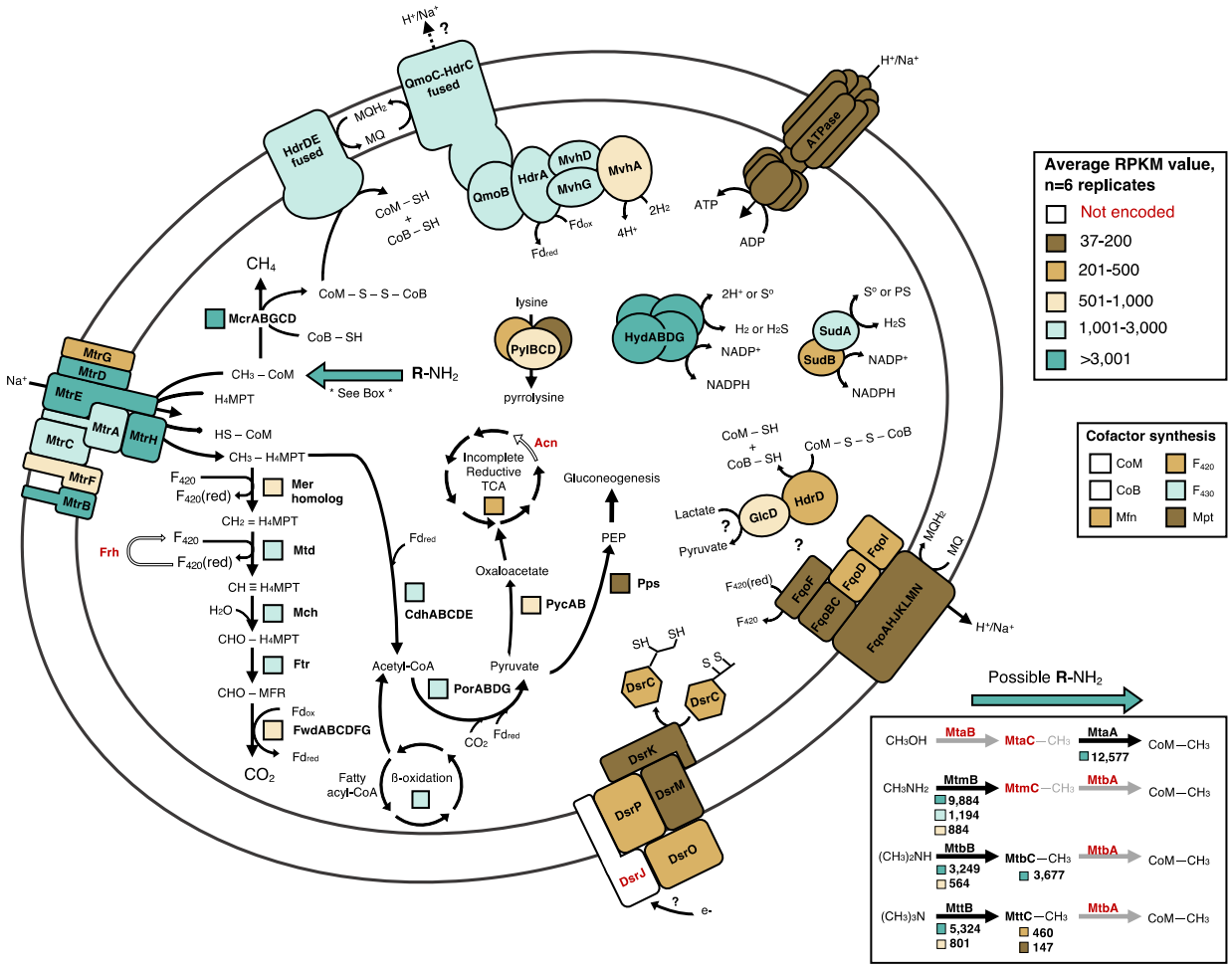

Fig. 5. Transcriptional activity in *Ca.* M. hypatiae grown under methanogenic conditions (N_2 headspace, 10 mM MMA, and 0.01% yeast extract). Transcriptionally active proteins are shown in bold black font. Proteins not encoded in the MAG are colored in white and denoted in bold red font. Average reads per kilobase of transcript per million mapped reads (RPKM) values of six biological replicates are depicted. RPKM values are represented by boxes or colored subunits close to each protein and are colored according to their expression level with the RPKM value of the lowest expressed gene depicted, 37 RPKM. For enzymes comprising multiple subunits, the beta-oxidation pathway, and the TCA cycle, an average RPKM value representing the transcribed enzymes is used. *Ca.* M. hypatiae is transcriptionally active under methanogenic conditions and encodes the ability to convert methyl-groups from mono-, di-, and trimethylamine to methane. This ability is enabled by several copies of substrate-specific methyltransferases and corrinoid proteins highlighted in the box to the bottom right. A complete list of genes described in this figure, their transcription levels, and their abbreviations is provided in Dataset S5.

Supporting Information

SI Results and Discussion

Protologue

Methanoglobus hypatiae sp. nov.

Me.tha.no.glo.bus. Gr. pref. *methano*-, pertaining to methane; L. masc. n. -*globus*, sphere; Gr.L. masc. n. *Methanoglobus*, methane producing organism spherical in shape. This genus was named by Buessecker *et al.* (1). Hy.pa.ti.ae. Gr. fem. hypatiae, to honor Hypatia of Alexandria, a respected and renowned philosopher of ancient Alexandria, Egypt, who made significant contributions to the understanding of mathematics and astronomy. A symbol of intellectual courage and scholarly achievement. This archaeon was cultured from an unnamed hot spring in the Lower Culex Basin of Yellowstone National Park identified as feature LCB024 (2). This archaeon is an obligately anaerobic thermophile that performs methylotrophic methanogenesis using methylamines and grows as regular to irregular coccoid cells approximately 0.5 to 1 µm in width. The type genome of this archaeon is deposited at NCBI under BioProject PRJNA1014417, accession number will be added upon publication.

SI Materials and Methods

Amplicon Sequencing and Analysis

DNA was extracted from environmental slurry samples and enrichment cultures sampled on the day of transfer using the FastDNA Spin Kit for Soil (MP Biomedicals, Irvine, CA) following the manufacturer's guidelines. Archaeal and bacterial 16S rRNA genes were amplified with the updated Earth Microbiome Project primer set 515F and 806R (3). Amplicon libraries were prepared as previously described (2) and sequenced by the Molecular Research Core Facility at Idaho State University (Pocatello, ID) using an Illumina MiSeq platform with 2 x 250 bp paired end read chemistry. Gene reads were processed using QIIME 2 version 2022.8 (4). Primer sequences were removed from demultiplexed reads using cutadapt (5) with error rate 0.12 and reads truncated (130 bp forward, 150 bp reverse), filtered, denoised and merged in DADA2 with default settings (6). Processed 16S rRNA gene amplicon sequence variants (ASVs) were taxonomically classified with the sklearn method and the SILVA 138 database (7). The R package *decontam* (version 1.18.0) (8) was used to remove contaminants using the "Prevalence" model with a threshold of 0.5.

Annotation and Reconstruction of Metabolic Potential

Genes associated with methanogenesis pathways, dissimilatory sulfur metabolism pathways, coenzyme and cofactor biosynthesis, energy conservation, and beta-oxidation, were inventoried. Annotations assigned by Prokka were refined through manual evaluation using KofamKOALA, NCBI BLASTP, NCBI's Conserved Domain Database, InterPro, the hydrogenase classifier HydDB, and DiSCo (9-14).

Phylogenetic and Phylogenomic Analyses

Average nucleotide identities (ANI) of 16S rRNA genes were calculated with blastn, while ANI and average amino acid identities (AAI) were calculated with pyani v02.2.12 (ANIb) and CompareM v0.0.23 (--fragLen 2000) (https://github.com/dparks1134/CompareM), respectively for selected Archaeoglobales genomes and MAGs (Table 1). Phylogenetic analysis of 16S rRNA genes was performed with fasttree (15) using masked alignments generated by ssu-align.

Phylogenomic analysis was performed with a concatenated muscle (16) alignments of 33 conserved phylogenetically informative single copy proteins (SI Appendix, Table S4) and maximum likelihood analysis with fasttree (WAG model). McrA alignments were performed with MAFFT-LINSi v7.522 (17), trimmed with trimAL v1.4.rev22 (18) using a 0.5 gap threshold, and maximum likelihood trees were built with IQTree2 v2.0.6 (19) using LG+C60+F+G model and 1,000 ultrafast bootstraps.

Temperature and Substrate Optimum Experiments

Methane production and growth of Archaeoglobus was evaluated at different temperatures and in the presence of methylated substrates (i.e., methanol and mono-, di-, and trimethylamine), lactate, and media prepared without yeast extract. The sixth transfer of the enrichment was used to inoculate triplicate 30 mL serum bottles containing 15 mL of medium with 8% v/v inoculum, streptomycin (50 mg/L), vancomycin (50 mg/L), and 10 mM of each substrate tested. Cultures were evaluated at 60 ˚C, 64 ˚C, 70 ˚C, 77 ˚C, 80 ˚C, and 85 ˚C with 10 mM MMA. Separately, we tested whether the culture would grow on the following substrate (combinations): 10 mM dimethylamine (DMA); 10 mM trimethylamine (TMA); 10 mM methanol (MeOH); 10 mM lactate (LAC); 10 mM MMA and 10 mM LAC); 10 mM MMA with media without yeast extract; and a control in media without yeast or any methanogenic substrate. The 70 ˚C cultures amended with 10 mM MMA served as the control. All incubations were performed in biological triplicate.

Methane Measurements

During cultivation, 250 µL subsamples of the headspace were taken using a gas tight syringe (Hamilton) and injected into a 10 mL autosampler vial that had been sealed with grey chlorobutyl septa. Samples were taken from the autosampler vials and injected into a Shimadzu 2020-GC gas chromatograph equipped with a GS433 CarbonPLOT column (30 m x 0.32 mm; 1.5 µm film thickness; Agilent) and a Rt-Q-BOND column (30 m x 0.32 mm; 1.5 µm film thickness; Restek) using helium as a carrier gas. The injector, column, and flame ionization detector (FID) were maintained at 200 ˚C, 50 ˚C, and 240 ˚C, respectively. Methane concentrations were calculated based on injection of a standard curve.

Fluorescence *in situ* hybridization and cell counts

Aliquots of enrichment cultures incubated with ^{13}C-MMA during the SIT experiment were treated with 2% paraformaldehyde (PFA) and fixed for 1 hr at room temperature. Following fixation, cells were washed twice with 1x PBS, followed by centrifugation at 16,000 × g to remove the supernatant, resuspended in 1x PBS, and stored at 4 ˚C. For direct cell counts, aliquots of fixed cell suspensions were filtered onto polycarbonate filters (0.2 µm pore size, 25 mm diameter, GTTP Millipore, Germany) and air dried before filter pieces were cut and embedded in 0.2% low melting agarose. We attempted to use the Archaeoglobales-specific probe Arglo32 (20), however fluorescent signal was insufficient. Given *Ca.* M. hypatiae was the sole archaeon in the enrichment culture, the relative abundance of *Ca.* M. hypatiae cells was determined via catalyzed reporter deposition fluorescence *in situ* hybridization (CARD-FISH) using the general archaea-targeted 16S rRNA oligonucleotide probe Arch915 (21). Total cell counts were based on DNA-stained cells using DAPI (4,6-diamidino-2-phenylindole). CARD-FISH was performed as previously described (22). Cell wall permeabilization was achieved with a brief treatment of 0.1 M HCl (1 min, RT) followed by treatment with 0.01 M HCl (15 min, RT). Endogenous peroxidases were inactivated with 0.15% H_2O_2 in methanol (30 min, RT). A formamide concentration of 35% was used for all hybridization reactions (2.5 hrs, 46˚C). CARD was performed using Alexa Fluor 594 labeled tyramides for 30 min at 46˚C. Following signal amplification, an additional washing step in 1x PBS was included to

reduce background fluorescence (15 min, RT, dark). Samples were stained with DAPI, embedded in Citifluor-Vectashield, and enumerated using an epifluorescence microscope (Leica DM4B).

Secondary electron microscopy

An aliquot of the enrichment culture at transfer 7 (T7) was treated with 2% paraformaldehyde (PFA) and fixed for 1 hr at room temperature. Following fixation, cells were washed twice through centrifugation at 16,000 × g to remove the supernatant, resuspended in 1x phosphate buffered saline (PBS), and stored at 4 ˚C. Samples for imaging were prepared according to Schaible et al., 2022 (23). Briefly, a square coupon of mirror-finished 304 stainless steel (25 mm diameter, 0.6 mm thickness) was purchased from Stainless Supply (Monroe, NC). The coupon was cleaned by washing with a 1% solution of Tergazyme (Alconox, New York, NY) and rinsed with Milli-Q water. The coupon was dried under compressed air and stored at room temperature. 5 µL of fixed sample was spotted on the coupon and air-dried at 46 °C for 3 min. The coupon was then dried for 1 m each step in a successive ethanol series starting with 10% ethanol and increasing by increments of 10% with the last step 90% ethanol. SEM images were captured using a Zeiss (Jena, Germany) SUPRA 55VP field emission scanning electron microscope (FE-SEM). The microscope was operated at 1 keV under a vacuum of 0.2–0.3 mPa, with a working distance of 5.4-6.2 mm at the Imagining and Chemical Analysis Laboratory (ICAL) of Montana State University (Bozeman, MT). No conductivity coating was applied before SEM analysis as the microscope was operated at 1 keV.

SI Detailed Author contributions

M.M.L. and R.H. developed the research project. M.M.L., Z.J.J., A.J.K, and R.H. designed experiments. M.M.L. and A.J.K. conducted field sampling. M.M.L. performed cultivation, extracted DNA for amplicon and metagenomic sequencing, extracted RNA for transcriptomic sequencing, and conducted physiology and stable isotope experiments. A.J.K. developed GC/GCMS protocols and processed GCMS samples. Z.J.J. processed and annotated metagenomic and transcriptomic data, assembled MAGs, mapped transcripts, assigned taxonomy, constructed 16S rRNA gene phylogeny, and performed phylogenetic analysis of MAGs. M.M.L. conducted phylogenetic analysis of amplicon data, refined gene annotations, reconstructed, and interpreted the metabolic potential of *Ca.* M. hypatiae with insight from Z.J.J and A.J.K. R.H. was responsible for funding and supervision of the project. M.M.L. and R.H. wrote the manuscript, which was then edited by all authors.

SI Tables

Table S1. Extended community composition history of methanogenic enrichment cultures via estimated relative abundance (%) from 16S rRNA gene amplicon sequencing.

	LCB024 sediment	Slurry 11/2021	Slurry 02/2022	Initial Enrichment	T1	T2	T3	T4	T4 - MG	T5	SIT-MG
Archaeoglobaceae ASV_78ad2	0.46	0.32	0.02	6.42	74.8	68.9	48.5	46.0	84.7	62.2	92.8
Pseudothermotoga ASV_17231	2.14	1.06	1.08	18.93	6.8	17.1	28.5	37.4	14.5	15.7	3.2
Other Archaeoglobaceae uncultured	0.00	0.00	0.00	1.54	0.0	0.01	0.0	0.0	0.0	0.0	0.0
Confirmed methanogenic archaea	0.25	0.38	0.45	0.00	0.0	0.0	0.0	0.0	0.0	0.0	0.0
Other Archaea	13.51	11.87	10.49	2.67	0.0	0.0	0.0	0.04	0.0	0.0	0.0
Other Bacteria	83.63	86.37	87.95	70.44	18.4	14.1	23.1	16.5	0.8	22.1	4.0

Table S2. Methane production of the enrichment culture over time. T, transfer.

Culture ID	Days continuous	Days	CH_4 (µM)	CH_4 (mM)	CH_4 (ppm)	CH_4 (%)
1A – initial enrichment	6	6	4.91	0.00	118.67	0.01
	13	13	16.73	0.02	404.73	0.04
	20	20	12.98	0.01	314.13	0.03
	27	27	12.86	0.01	311.20	0.03
	36	36	32.92	0.03	796.48	0.08
	48	48	146.28	0.15	3538.80	0.35
	53	53	279.15	0.28	6753.17	0.68
	63	63	419.11	0.42	10139.33	1.01
	70	70	447.12	0.45	10816.36	1.08
T1	82	12	14.40	0.01	348.40	0.03
	91	21	50.85	0.05	1230.06	0.12
	98	27	198.41	0.20	4800.09	0.48
	106	35	390.47	0.39	9445.97	0.94
	113	42	565.32	0.57	13676.04	1.37
	117	46	688.44	0.69	16654.06	1.67
	126	55	1442.03	1.44	34885.74	3.49
	133	62	1844.13	1.84	44611.75	4.46
T2	146	7	15.22	0.02	368.32	0.04
	158	18	16.11	0.02	389.83	0.04
	175	34	49.40	0.05	1195.06	0.12
	197	57	680.54	0.68	16463.41	1.65
	221	81	2200.24	2.20	53227.90	5.32
	229	89	2654.34	2.65	64213.66	6.42
	238	98	2230.72	2.23	53964.66	5.40
T3	243	5	18.17	0.02	439.53	0.04
	259	21	10.70	0.01	258.82	0.03
	266	28	536.13	0.54	12969.71	1.30
	274	36	2413.23	2.41	58379.47	5.84
	280	42	2283.95	2.28	55253.34	5.53
	284	46	2193.96	2.19	53077.04	5.31
T4	294	10	17.36	0.02	420.07	0.04
	301	17	18.12	0.02	438.37	0.04
	309	25	12.51	0.01	302.54	0.03
	319	35	1944.01	1.94	47028.08	4.70
	327	43	3054.00	3.05	73881.94	7.39
	335	51	2619.45	2.62	63370.12	6.34
T5	347	10	13.41	0.01	324.42	0.03
	355	18	13.14	0.01	317.78	0.03
	365	28	137.59	0.14	3328.60	0.33
	371	34	1023.35	1.02	24756.27	2.48
	375	38	2218.75	2.22	53674.81	5.37
	384	46	2459.29	2.46	59493.85	5.95
T6	386	2	16.29	0.02	394.19	0.04
	393	9	21.33	0.02	516.14	0.05
	400	16	18.68	0.02	451.92	0.05
	407	23	245.86	0.25	5947.76	0.59
	412	28	2555.27	2.56	61815.61	6.18
	414	30	3432.93	3.43	83051.24	8.31
	416	32	3621.90	3.62	87623.79	8.76
	418	34	3942.97	3.94	95385.88	9.54
T7	428	9	34.33	0.03	830.38	0.08
	435	16	296.91	0.30	7182.55	0.72
	440	21	2931.05	2.93	70907.06	7.09
	444	25	3164.45	3.16	76553.52	7.66
	446	27	3338.04	3.34	80751.55	8.08

Table S3. Extended Archaeoglobales metagenome assembled genome and isolate genome statistics. A combined assembly of metagenomes from T4-MG and SIT-MG (Fig. 1A) for the *Ca.* M. hypatiae LCB24 MAG was used as it yielded an improved assembly. Len., length; Compl., completeness; Redun, redundancy; Strain Hetero., strain heterogeneity; pOGT, predicted optimal growth temperature. [*] stop codon interrupts *mcrA* sequence; [a] Both sequences 5′ start; not identical; [b] Consists of 1 chromosome and 1 plasmid.

	Seqs	Len (Mb)	GC (%)	Compl. (%)	Redun. (%)	16S	tRNA	CDS	*mcrA*	CRISPRs	pOGT (°C)	Citation
***Ca.* M. hypatiae LCB24**	19	1.624	46.12	100	1.31	1	44	1,760	1	2	74.44	This study
Archaeoglobales LCB024-003	179	1.157	45.72	88.48	1.31	0	31	1,226	1	1	73.90	Lynes, Krukenberg et al, 2023
Archaeoglobales WYZ-LMO2	220	1.514	45.92	97.6	0	0	40	1,614	1	2	72.40	Wang 2019
Archaeoglobales bin74	127	1.547	45.63	92.81	1.31	1	34	1,679	0[*]	9	75.32	Liu 2020
Archaeoglobales SJ3.Bin34	73	1.468	46.00	98.69	0.65	0	39	1,581	1	2	73.13	Colman 2019
Ca. Methanoglobus nevadensis GBS	71	1.602	47.16	98.04	3.66	1	47	1,785	1	2	74.75	Peacock 2013
Archaeoglobales GMQP bin32	20	1.727	41.26	100	0.98	1	39	1,931	1	2	71.88	Hua 2019
Archaeoglobales GMQP_D bin 18	22	1.565	42.01	97.39	0.98	1	45	1,747	1	3	69.41	Wang 2023
Archaeoglobales JZ-3 D bin 138	32	1.550	42.08	99.35	1.31	1	43	1,701	1	2	69.11	Wang 2023
Archaeoglobales WYZ-LMO1	140	1.557	43.85	88.89	1.31	1	41	1,701	1	1	72.72	Wang 2019
Archaeoglobales WYZ-LMO3	135	1.568	43.93	88.03	1.96	2[a]	35	1,670	1	2	73.09	Wang 2019
Archaeoglobales bin11	252	1.220	47.59	91.83	6.17	1	27	1,387	1	0	72.64	Liu 2020
Archaeoglobales bin16	46	1.668	45.49	96.51	1.31	0	41	1,864	1	2	72.69	Liu 2020
Archaeoglobus JZ bin24	35	1.492	44.66	99.35	1.31	0	44	1,642	0	2	68.52	unpublished
Archaeoglobales LCB024-002	66	1.334	42.28	97.39	0.03	0	41	1,459	0	0	73.46	Lynes et al, 2023
Archaeoglobales LCB003-04	128	1.335	42.27	96.73	1.96	0	38	1,447	0	0	73.71	Lynes et al, 2023
Archaeoglobales SJ3.bin61	45	1.270	41.68	89.54	0	1	40	1,392	0	0	73.34	Colman 2019
Archaeoglobales JZ_75 SW bin 109	16	1.562	39.48	99.35	0.65	1	45	1,762	1	5	74.34	Wang 2023
Archaeoglobus fulgidus DSM 4304	1	2.178	48.58	100	0	1	46	2,440	0	3	79.88	Klenk 1997
Archaeoglobus neptunius SE56	32	2.116	46.05	100	0	1	47	2,336	0	2	78.26	Slobodkina 2021
Archaeoglobus profundus DSM 5631	2[b]	1.563	46.05	100	0	1	48	1,784	0	0	85.86	von Jan 2010
Ferroglobus placidus DSM 10642	1	2.196	44.14	100	0	1	49	2,467	0	1	83.83	Anderson 2011
Geoglobus acetivorans SBH6	1	1.861	46.84	99.84	0	1	48	2,168	0	6	78.22	Mardanov 2014
Geoglobus ahangari 234	1	1.770	53.11	100	0	1	46	1,985	0	7	84.11	Manzella 2015
Archaeoglobus sulfaticallidus PM70-1	1	2.077	43.24	100	0	1	51	2,237	0	1	76.12	Stokke 2013
Archaeoglobus veneficus SNP6	1	1.902	47.05	99.35	0	1	46	2,055	0	2	76.18	Mukherjee 2017
Polytropus marinifundus rG16	21	2.129	40.22	99.84	1.96	1	44	2,286	2	0	66.39	Boyd 2019

Table S4. Conserved single copy proteins used in phylogenomic analysis of MAGs and isolates.

arCOG	Gene	Product
arCOG00405	GRS1	Glycyl-tRNA synthetase (class II)
arCOG00779	RplO	Ribosomal protein L15
arCOG00785	RpmC	Ribosomal protein L29
arCOG01001	Map	Methionine aminopeptidase
arCOG01183	Kae1p/TsaD	Subunit of KEOPS complex, contains a domain with ASKHA fold and RIO-type kinase (AP-endonuclease activity)
arCOG01228	Ffh	Signal recognition particle GTPase
arCOG01722	RpsM/rps13p	Ribosomal protein S13
arCOG01758	RpsJ/rps10p	Ribosomal protein S10
arCOG04070	RplC	Ribosomal protein L3
arCOG04071	RplD	Ribosomal protein L4
arCOG04072	RplW	Ribosomal protein L23
arCOG04086	RpmD	Ribosomal protein L30
arCOG04087	RpsE	Ribosomal protein S5
arCOG04088	RplR	Ribosomal protein L18
arCOG04090	RplF/rpl6p	Ribosomal protein L6P
arCOG04091	RpsH/rps8p	Ribosomal protein S8
arCOG04094	RplX/rpl24p	Ribosomal protein L24
arCOG04095	RplN/rps14p	Ribosomal protein L14
arCOG04096	RpsQ/rps17p	Ribosomal protein S17
arCOG04097	RpsC/rps3p	Ribosomal protein S3
arCOG04098	RplV/rpl22p	Ribosomal protein L22
arCOG04113	RplP	Ribosomal protein L10AE/L16
arCOG04121	RnhB	Ribonuclease HII
arCOG04169	SecY	Preprotein translocase subunit SecY
arCOG04185	RpsO	Ribosomal protein S15P
arCOG04239	RpsD/rps4p	Ribosomal protein S4 or related protein
arCOG04242	RplM/rpl13p	Ribosomal protein L13
arCOG04243	RpsI/rps9p	Ribosomal protein S9
arCOG04245	RpsB/rps2p	Ribosomal protein S2
arCOG04255	RpsL/rps12p	Ribosomal protein S12
arCOG04256	RpoC/Rpo11	DNA-directed RNA polymerase subunit A"
arCOG04257	RpoC/Rpo3/rpoA1	DNA-directed RNA polymerase subunit A'
arCOG04277	Efp	Translation elongation factor P (EF-P)/translation initiation factor 5A (eIF-5A)

Table S5. Calculated cell density of replicates in the SIT experiment. FID measurements of replicates used to determine cell density. Density is calculated based on cell counts of DAPI and CARD-FISH labeled samples. Stdev., standard deviation. Letters A-F identify each replicate.

Summary	**$^{12}CH_4$**		**Cell Density, cells mL^{-1}**		
Replicate ID	**µM**	**ppm**	**DAPI**	**FISH**	**% labeled with Arch915**
5A Day 22	25	610	3.83×10^7	1.34×10^6	3.5
5B Day 22	57	1,374	1.88×10^7	5.07×10^6	12.7
5E Day 22	50	1,204	3.49×10^7	0	0
5F Day 22	132	3,196	4.59×10^7	2.21×10^6	4.8
Day 22 Average	66	1,596	3.45×10^7	2.16×10^6	5.3
Day 22 Stdev.	46	1,116	1.14×10^7	2.15×10^6	5.4
5A Day 32	741	17,917	4.26×10^7	2.85×10^7	66.9
5B Day 32	2,176	52,635	1.11×10^8	6.00×10^7	54.2
5E Day 32	1,779	43,035	3.40×10^7	1.74×10^7	51.2
5F Day 32	2,412	58,355	9.14×10^7	4.03×10^7	44.1
Day 32 Average	1,777	42,985	6.97×10^7	3.65×10^7	54.1
Day 32 Stdev.	739	17,868	3.73×10^7	1.82×10^7	9.6
5A Day 45	4,109	99,398	12.2×10^7	6.41×10^7	52.7

SI Figures

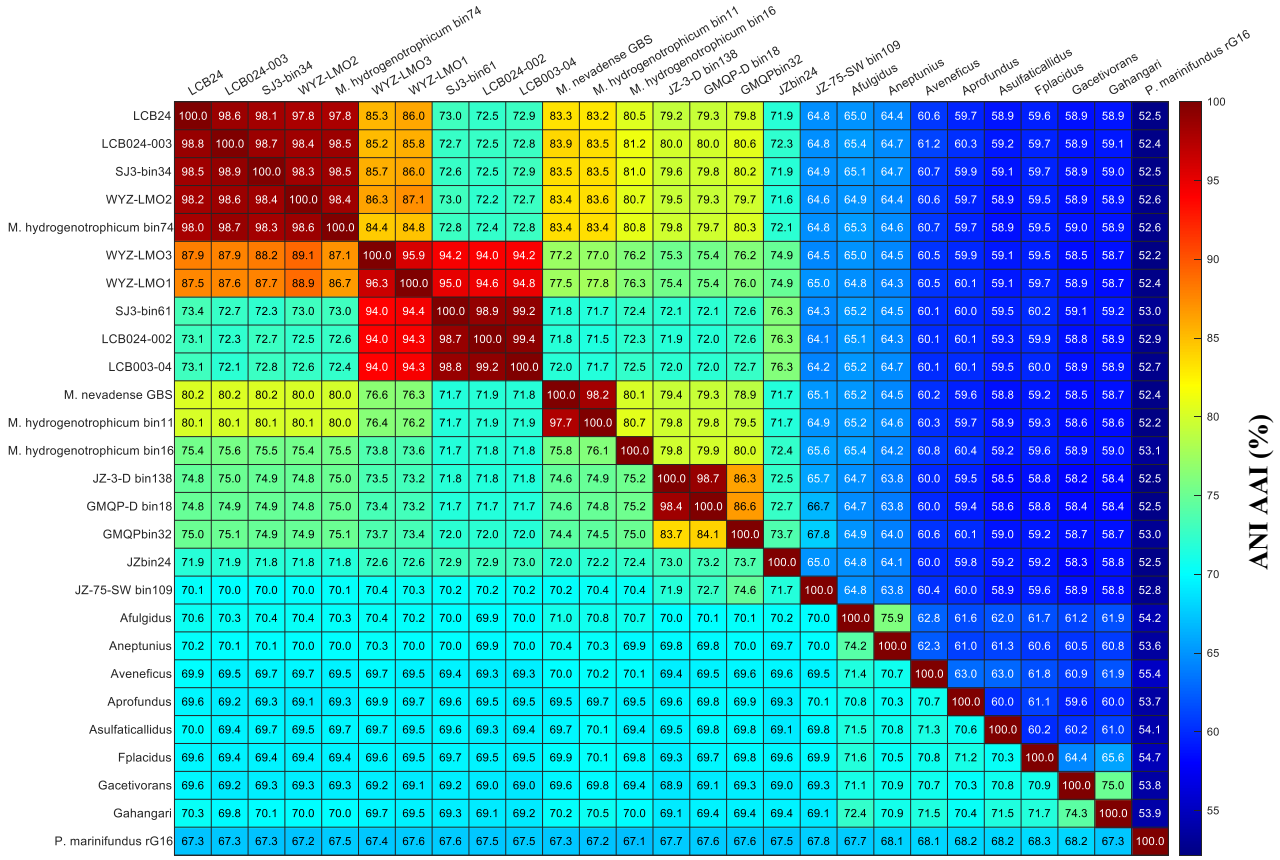

Fig. S1. Detailed ANI (lower half of matrix) and AAI (upper half of matrix) analysis of related Archaeoglobales MAGs and reference genomes.

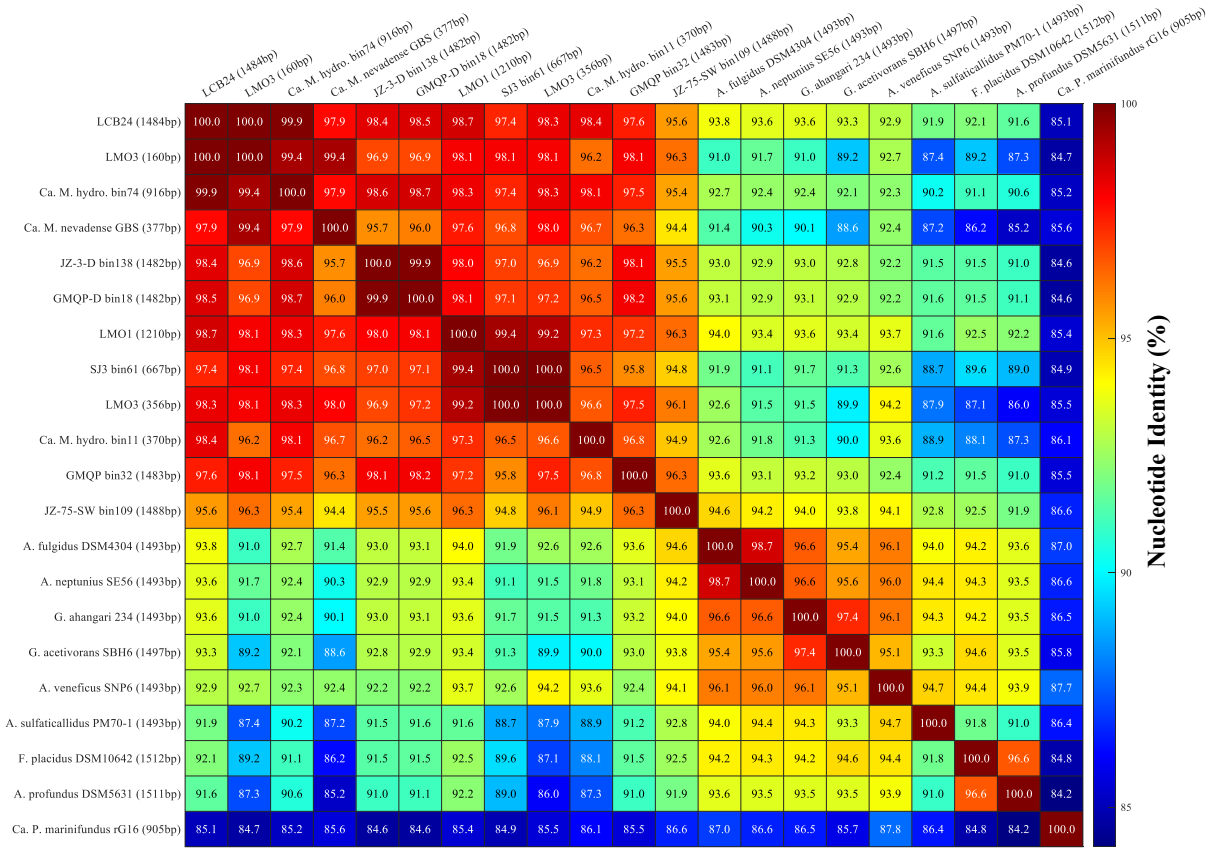

Fig. S2. 16S rRNA nucleotide identity analysis of closely related Archaeoglobales MAGs and reference genomes.

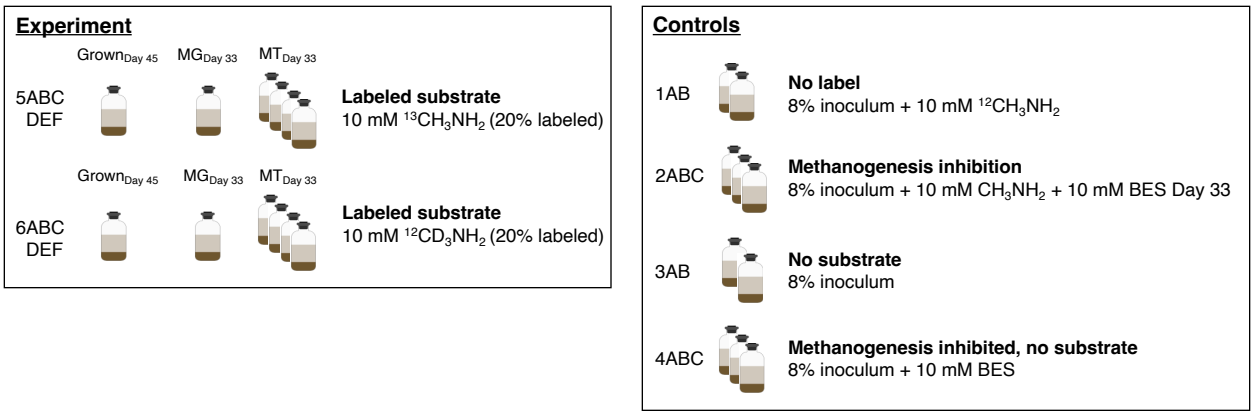

Fig. S3. Experimental setup of the stable isotope tracing (SIT) experiment. Replicates sacrificed for analysis during mid-log phase are indicated. Of the eight samples harvested for metatranscriptomics, six were sequenced and used for analysis as two replicates did not yield sufficient RNA for sequencing. MG, metagenome sample; MT, metatranscriptome sample; BES, bromoethanesulfonate/methanogenesis inhibitor.

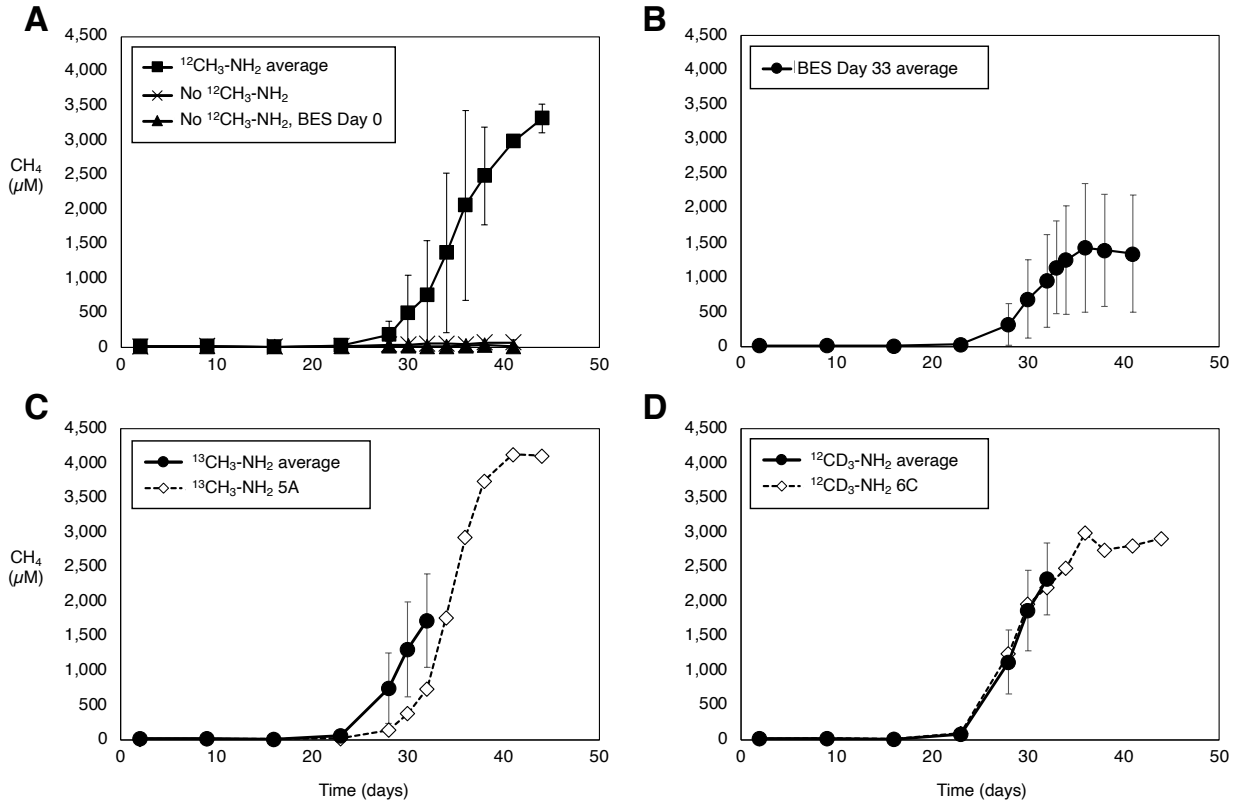

Fig. S4. $^{12}CH_4$ measurements by GC-FID during the stable isotope tracing experiment. Measurements can be found in Dataset S3.

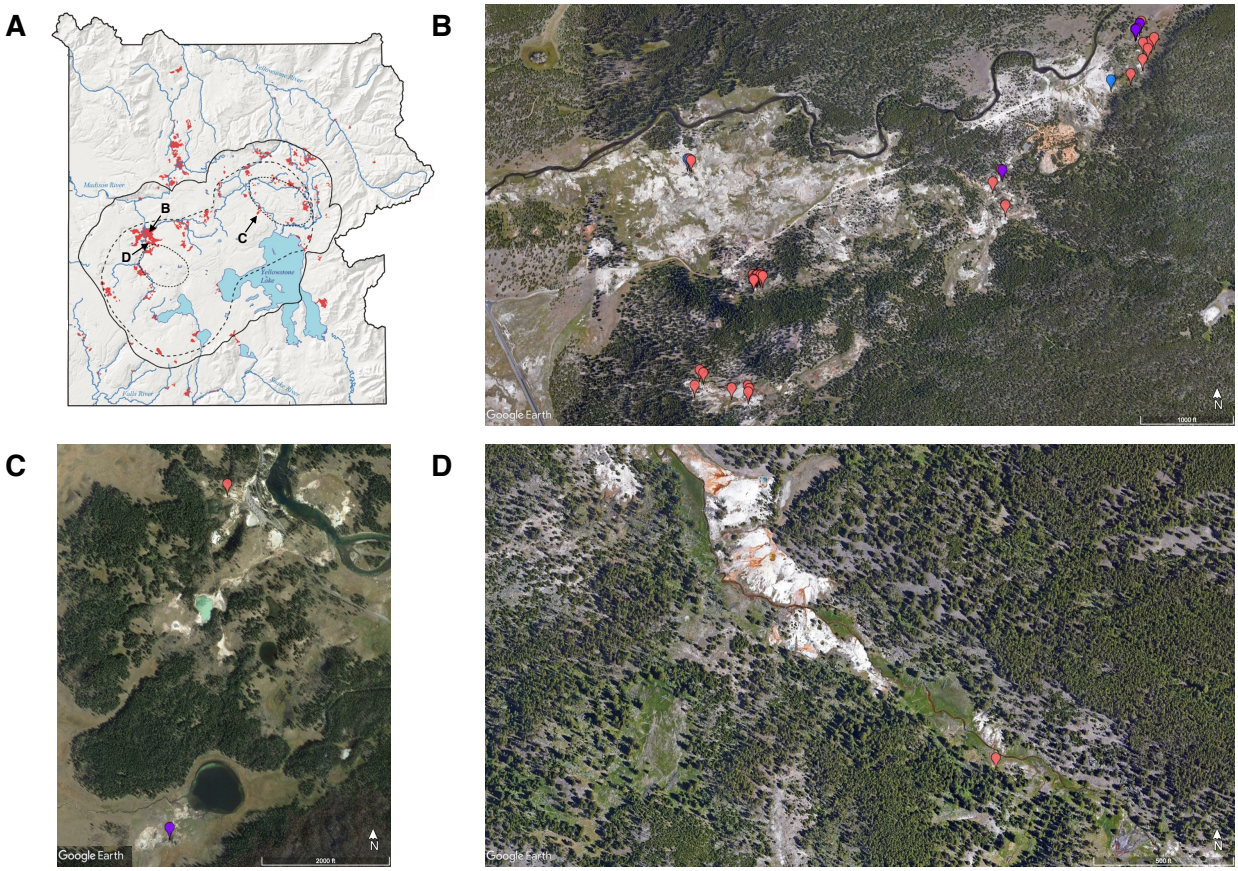

Fig. S5. Geographical distribution of geothermal features in Yellowstone National Park in which Archaeoglobi-related *mcrA* genes (n = 36) and *Ca.* M. hypatiae-related 16S rRNA genes (n = 6) were detected. Features are located in the (*A*) Map of Yellowstone National Park Wyoming, USA modified from Vaughan *et al.* 2014 (24) *(B)* Lower Culex Basin (n = 36), (*C*) Mud Volcano Region (n = 2), and (*D*) the White Creek Area (n = 1). These features spanned a wide pH (2.61-9.35) and temperature (18.4-93.8 ºC) range. Features in which *mcrA* were detected are marked in red, while features with related 16S rRNA genes are shown in blue. Features in which both amplicons were detected are colored in purple. For details on these sites, their *mcrA* data, water geochemistry, and exact location, see Lynes & Krukenberg et al., 2023. Image source: Google Earth.

Description of Available Supplementary Datasets

SI Dataset S1. Extended metagenome assembled genome (SIT-MG) and isolate genome statistics. Seqs, sequences; avg_cov, average coverage; avg_gc, average G+C content; % rel. abund., percent relative abundance.

SI Dataset S2. GCMS measurements of masses 16 (CH_4), 17 ($^{13}CH_4$), and 19 ($^{12}CD_3H$) during the isotope tracing experiment. Percent of labeled methane is calculated as a fraction of provided labeled substrate. Stdev, standard deviation.

SI Dataset S3. Gas chromatograph FID measurements of $^{12}CH_4$ during isotope tracing experiment. NA, not available/measured.

SI Dataset S4. Gas chromatograph FID measurements of CH_4 during temperature optimum experiment. NA, not available/measured.

SI Dataset S5. Inventory of genes expressed by *Ca.* M. hypatiae LCB24 under methanogenic conditions and as depicted in Fig. 5. Expression levels averaged across six replicates are reported in reads per kilobase of transcript per million mapped reads (RPKM).

References

1. S. Buessecker *et al.*, Mcr-dependent methanogenesis in Archaeoglobaceae enriched from a terrestrial hot spring. *The ISME Journal* 10.1038/s41396-023-01472-3 (2023).
2. M. M. Lynes *et al.*, Diversity and function of methyl-coenzyme M reductase-encoding archaea in Yellowstone hot springs revealed by metagenomics and mesocosm experiments. *ISME Communications* **3**, 22 (2023).
3. A. Apprill, S. McNally, R. Parsons, L. Weber, Minor revision to V4 region SSU rRNA 806R gene primer greatly increases detection of SAR11 bacterioplankton. *Aquatic microbial ecology : international journal* **75**, 129-137 (2015).
4. E. Bolyen *et al.*, Reproducible, interactive, scalable and extensible microbiome data science using QIIME 2. *Nature Biotechnology* **37**, 852-857 (2019).
5. M. Martin, Cutadapt removes adapter sequences from high-throughput sequencing reads. *2011* **17**, 3 (2011).
6. B. J. Callahan *et al.*, DADA2: High-resolution sample inference from Illumina amplicon data. *Nat Methods* **13**, 581-583 (2016).
7. C. Quast *et al.*, The SILVA ribosomal RNA gene database project: improved data processing and web-based tools. *Nucleic Acids Research* **41**, D590-D596 (2012).
8. N. M. Davis, D. M. Proctor, S. P. Holmes, D. A. Relman, B. J. Callahan, Simple statistical identification and removal of contaminant sequences in marker-gene and metagenomics data. *Microbiome* **6**, 226 (2018).
9. T. Aramaki *et al.*, KofamKOALA: KEGG Ortholog assignment based on profile HMM and adaptive score threshold. *Bioinformatics* **36**, 2251-2252 (2019).
10. S. Lu *et al.*, CDD/SPARCLE: the conserved domain database in 2020. *Nucleic Acids Res* **48**, D265-D268 (2020).
11. D. Sondergaard, C. N. Pedersen, C. Greening, HydDB: A web tool for hydrogenase classification and analysis. *Sci Rep* **6**, 34212 (2016).
12. M. Blum *et al.*, The InterPro protein families and domains database: 20 years on. *Nucleic Acids Research* **49**, D344-D354 (2020).
13. S. Neukirchen, F. L. Sousa, DiSCo: a sequence-based type-specific predictor of Dsr-dependent dissimilatory sulphur metabolism in microbial data. *Microb Genom* **7** (2021).
14. S. Neukirchen, F. L. Sousa, DiSCo: a sequence-based type-specific predictor of Dsr-dependent dissimilatory sulphur metabolism in microbial data. *Microbial Genomics* **7** (2021).
15. M. N. Price, P. S. Dehal, A. P. Arkin, FastTree 2--approximately maximum-likelihood trees for large alignments. *PLoS One* **5**, e9490 (2010).
16. R. C. Edgar, MUSCLE: multiple sequence alignment with high accuracy and high throughput. *Nucleic Acids Res* **32**, 1792-1797 (2004).
17. K. Katoh, D. M. Standley, MAFFT Multiple Sequence Alignment Software Version 7: Improvements in Performance and Usability. *Molecular Biology and Evolution* **30**, 772-780 (2013).
18. S. Capella-Gutiérrez, J. M. Silla-Martínez, T. Gabaldón, trimAl: a tool for automated alignment trimming in large-scale phylogenetic analyses. *Bioinformatics* **25**, 1972-1973 (2009).
19. B. Q. Minh *et al.*, IQ-TREE 2: New Models and Efficient Methods for Phylogenetic Inference in the Genomic Era. *Molecular Biology and Evolution* **37**, 1530-1534 (2020).

20. A. Rusch, J. P. Amend, Order-specific 16S rRNA-targeted oligonucleotide probes for (hyper) thermophilic archaea and bacteria. *Extremophiles* **8**, 357-366 (2004).
21. D. A. Stahl, Development and application of nucleic acid probes in bacterial systematics. *Nucleic Acid Techniques in Bacterial Systematics*, 205-248 (1991).
22. A. Pernthaler, J. Pernthaler, R. Amann, Fluorescence in situ hybridization and catalyzed reporter deposition for the identification of marine bacteria. *Applied and environmental microbiology* **68**, 3094-3101 (2002).
23. G. A. Schaible, A. J. Kohtz, J. Cliff, R. Hatzenpichler, Correlative SIP-FISH-Raman-SEM-NanoSIMS links identity, morphology, biochemistry, and physiology of environmental microbes. *ISME Communications* **2**, 52 (2022).
24. R. G. Vaughan, H. P. Heasler, C. Jaworowski, J. B. Lowenstern, L. P. Keszthelyi, *Provisional maps of thermal areas in Yellowstone National Park based on satellite thermal infrared imaging and field observations* (US Department of the Interior, US Geological Survey, 2014).